A multimodel evaluation of the potential impact of shipping on particle species in the Mediterranean Sea

Lea Fink[1], Matthias Karl[1], Volker Matthias[1], Sonia Oppo[2], Richard Kranenburg[3], Jeroen Kuenen[3], Sara Jutterström[4], Jana Moldanova[4], Elisa Majamäki[5], Jukka-Pekka Jalkanen[5]

[1]Helmholtz-Zentrum Hereon, Institute of Coastal Environmental Chemistry, 21502 Geesthacht, Germany
[2]AtmoSud, Air Quality Observatory in the Provence-Alpes-Côte d'Azur region, 13006 Marseille, France
[3]TNO, Netherlands Organization for Applied Scientific Research, 3584 CB Utrecht, The Netherlands
[4]IVL, Swedish Environmental Research Institute, 411 33 Göteborg, Sweden
[5]FMI, Finnish Meteorological Institute, FI-00560 Helsinki, Finland

Correspondence to: Lea Fink (lea.fink@hereon.de)

Abstract. Shipping contributes significantly to air pollutant emissions and atmospheric particulate matter (PM) concentrations. At the same time, worldwide maritime transport volumes are expected to continue to rise in the future. The Mediterranean Sea is a major short-sea shipping route within Europe, as well as the main shipping route between Europe and East Asia. As a result, it is a heavily trafficked shipping area, and air quality monitoring stations in numerous cities along the Mediterranean coast have detected high levels of air pollutants originating from shipping emissions.

The current study is a part of the EU Horizon 2020 project SCIPPER (Shipping contribution to Inland Pollution - Push for the Enforcement of Regulations) which intends to investigate how existing restrictions on shipping-related emissions to the atmosphere ensure compliance with legislation. To demonstrate the impact of ships on relatively large scales, the potential shipping impacts on various air pollutants can be simulated with chemistry transport models.

To determine formation, transport, chemical transformation and fate of $PM_{2.5}$ in the Mediterranean Sea in 2015, five different regional chemistry transport models (CAMx – Comprehensive Air Quality Model with Extensions, CHIMERE, CMAQ – Community Multiscale Air Quality model, EMEP – European Monitoring and Evaluation Programme model, LOTOS-EUROS) were applied. Furthermore, $PM_{2.5}$ precursors (NH_3, SO_2, HNO_3) and inorganic particle species (SO_4^{2-}, NH_4^+, NO_3^-) were studied, as they are important for explaining differences among the models. STEAM version 3.3.0 was used to compute shipping emissions, and the CAMS-REG v2.2.1 dataset was used to calculate land-based emissions for an area encompassing the Mediterranean Sea at a resolution of 12×12 km^2 (or $0.1° \times 0.1°$). For additional input, like meteorological fields and boundary conditions, all models utilized their regular configuration. The zero-out approach was used to quantify the potential impact of ship emissions on $PM_{2.5}$ concentrations. The model results were compared to observed background data from monitoring sites.

Four of the five models underestimated the actual measured $PM_{2.5}$ concentrations. These underestimations are linked to model-specific mechanisms or underpredictions of particle precursors. The potential impact of ships on the $PM_{2.5}$ concentration is

between 15 % and 25 % at the main shipping routes. Regarding particle species, SO_4^{2-} is main contributor to the absolute ship-related $PM_{2.5}$ and to total $PM_{2.5}$ concentrations. In the ship-related $PM_{2.5}$, a higher share of inorganic particle species can be found when compared to the total $PM_{2.5}$. The seasonal variabilities in particle species show that NO_3^- is higher in winter and spring, while the NH_4^+ concentrations displayed no clear seasonal pattern in any models. In most cases with high concentrations of both NH_4^+ and NO_3^-, lower SO_4^{2-} concentrations are simulated. Differences among the simulated particle species distributions might be traced back to the aerosol size distribution and how models distribute emissions among the coarse and fine mode ($PM_{2.5}$ and PM_{10}). The seasonality of wet deposition follows the seasonality of the precipitation, displaying that precipitation predominates the wet deposition.

List of Abbreviations

1.5-D	1.5-dimensional
CAMx	Comprehensive Air Quality Model with Extensions
CMAQ	Community Multiscale Air Quality model
CTM	Chemistry Transport Model
EEA	European Environment Agency's
EMEP	European Monitoring and Evaluation Programme model
GNFR	Gridded Nomenclature for Reporting
MARS	Model for an Aerosol Reacting System
MEPC	Marine Environment Protection Committee
NMB	Normalized mean bias
NMVOC	Non-methane volatile organic compound
PM	particulate matter
POA	primary organic aerosol
PSAT	Particulate Source Apportionment Technology
R	Spearman's correlation coefficient
RADM-AQ	Regional Acid Deposition Model−Aqueous Chemistry
RMSE	root mean square error
SCIPPER	Shipping contribution to Inland Pollution - Push for the Enforcement of Regulations
SOAP	Secondary Organic Aerosol Processor
SOAs	Secondary organic aerosol
STEAM	Ship Traffic Emission Assessment Model
CBM-IV	Carbon bond mechanism (version IV)
TPPM	Total primary particulate matter

VBS   volatility basis set

VOC   volatile organic compound

1 Introduction

Exhaust particles emitted from shipping have a large share in total emissions from the transport sector (Corbett and Fischbeck,
70 1997; Eyring et al., 2005), thereby affecting the chemical composition of the atmosphere as well as the regional air quality. Particularly in coastal areas, maritime transport contributes a considerable fraction to air pollution (Viana et al., 2014). High $PM_{2.5}$ concentrations can be caused by transported particles, desert dust or the production of secondary particulate matter (Tomasi et al., 2017). Previous studies have revealed that in Europe, the $PM_{2.5}$ (particulate matter < 2.5 μm) concentration increase caused by shipping emissions is small (Viana et al., 2009; Aksoyoglu et al., 2016). Nevertheless, in the Mediterranean
75 region the relative ship impact on the $PM_{2.5}$ concentration is large, with a share of 5 % to 20 % of the total $PM_{2.5}$ concentration (e.g., Aksoyoglu et al. 2016, Nunes et al., 2020). Especially the formation of secondary particulate matter from ship emissions is of importance. According to Viana et al. (2009), the secondary contribution of ship emissions is equivalent to double their primary contribution. Secondary particles in the atmosphere form from gaseous precursors, whereas primary particles are directly emitted and evolve within a short time to form secondary particles. To improve the air quality in coastal regions, it is
80 important to identify the pollutant sources and make reliable estimations of their impacts on surrounding PM levels. It has been shown that the majority of secondary particles contributing to local PM in ports come from shipping (Song & Shon, 2014). Furthermore, according to Klimont et al. (2017), the proportion of international shipping's particulate matter primary emissions to global anthropogenic emissions is between 3% and 4%, which is comparable to road traffic. Additionally, shipping contributions to total $PM_{2.5}$ concentrations far from coastlines were found to be responsible for exceedances of WHO
85 air quality guideline values (Nunes et al., 2020). The annual mean $PM_{2.5}$ limit value in the EU is 25 μg/m³ (EU DIRECTIVE 2008/50/EC, 2008), whereas the annual mean $PM_{2.5}$ goal established by the WHO is 5.0 μg/m³ (WHO, 2021). Strong evidence was found between exposure to $PM_{2.5}$ and the occurrences of certain diseases affecting the lungs, cancer, or type 2 diabetes (Heusinkveld et al., 2016; Chen et al., 2016; Gao and Sang, 2020). According to the WHO, there is no safe level of $PM_{2.5}$; thus, the gap between the WHO and EU $PM_{2.5}$ values is of actual concern (Karamfilova, 2022).
90 The MEPC decided in December 2022 to establish a sulfur emission control area in the Mediterranean Sea by 1st January 2025. In this area, the limit for sulfur in fuel oils used on board ships is 0.10 % (IMO, 2022). The global sulfur cap for marine vessels came into effect in January 2020, which declares that the sulfur content of any fuel oil used from ships must not exceed 0.50 % m/m, except for ships using 'equivalent' compliance mechanisms, such as scrubbers. Calculations show that this policy has led to $PM_{2.5}$ reductions ranging from 0.5 μg/m³ to more than 2.0 μg/m³ along the major shipping routes in the Mediterranean
95 Sea (Jonson et al., 2020). These relatively strict 2020 regulations are expected to lower the number of $PM_{2.5}$-related premature deaths by on average 15% (Viana et al., 2020).

Although the Mediterranean Sea contains one of the busiest shipping routes worldwide only a few regional-scale chemistry transport modeling studies have considered this region. Viana et al. (2014) reviewed studies concerning the impacts of shipping emissions on air quality in European coastal areas, noting that the highest $PM_{2.5}$ contributions were found in the Mediterranean Sea and North Sea. Aksoyoglu et al. (2016) studied $PM_{2.5}$ concentrations in the Mediterranean Sea followed up by a comparison of two models. Marmer and Langmann (2005) investigated the Mediterranean Sea on a broader scale and without comparing different CTM systems. Nevertheless, other studies have concentrated on smaller domains, such as the Iberian Peninsula (Baldasano et al., 2011; Nunes et al., 2020), the eastern Mediterranean Sea with the Arabian Peninsula (Večeřa et al., 2008; Tadic et al., 2020; Celik et al. 2020; Friedrich et al., 2021), or urban scale and harbor cities (Schembari et al., 2012; Donateo et al., 2014; Prati et al., 2015). None of these studies, however, analyzed the potential shipping impacts on $PM_{2.5}$ concentrations together with individual aerosol species on a regional basis, additionally comparing the results of five CTMs.

A wide range of gaseous pollutants, such as sulfur dioxide (SO_2) and nitrogen oxide ($NO_x = NO + NO_2$), coming from shipping emissions can be precursors for particle formation (Jägerbrand et al., 2019; Karl et al., 2019; Matthias et al., 2010). Sulfur dioxide is released mainly by human activities such as fossil fuel burning, petroleum refining, and metal smelting (Zhong et al., 2020). SO_2 is oxidized by dissolved oxidants such as O_3 and hydrogen peroxide (H_2O_2) in the aqueous phase and by OH in the gas phase to generate H_2SO_4 (Seinfeld and Pandis, 2006). H_2SO_4 and HNO_3 react with NH_3 to form ammonium sulfate (($NH_4)_2SO_4$) and NH_4NO_3 aerosols, with H_2SO_4 neutralization having preference due to its lower vapor pressure (Hauglustaine et al., 2014).

Nitrogen oxides are primarily removed during the day via the hydroxyl (OH) radical oxidation reaction to produce nitric acid (HNO_3; Seinfeld and Pandis, 1998). At night, the main NO_x removal method involves interacting with ozone (O_3) to produce the nitrate (NO_3) radical, which then may combine with nitrogen dioxide (NO_2) to form dinitrogen pentoxide (N_2O_5) and subsequently may undergo a heterogeneous reaction with water to produce HNO_3. As it is highly soluble, HNO_3 disperses quickly in water droplets or is neutralized by reaction with ammonia (NH_3) to produce NH_4NO_3 aerosols. Increased emissions of NH_3 or HNO_3 formation as well as their deposition negatively affect the environment through eutrophication and acidification, thereby contributing to the loss of ecosystem biodiversity (Remke et al., 2009; Kleijn et al.; 2009; Krupa, 2003). Furthermore, the air pollution status should be assessed to investigate the consequences of new legislation.

The current work investigates and analyzes the predictions of five different CTMs for air pollutant dispersion and transformation. The intercomparison was carried out in two parts: Part one included the photochemistry and differences among the models regarding NO2 and O3 (Fink et al., 2023). The present study is part two of the model intercomparison and evaluates the same CTM simulations but different air pollutants, namely aerosols. This paper is structured as followed: Sect. 3.1 and 3.2 considers simulated overall $PM_{2.5}$ model performance and spatial distribution. In Sect. 3.3, precursors (NH_3, HNO_3, SO_2 and NO_2) are investigated, as a base for inorganic particle species. Inorganic aerosols concentration and wet deposition is regarded in Sect. 3.4.

To date, the present study is the first multimodel study designed to compare the potential impacts of shipping on $PM_{2.5}$ and particle species simulated by five regional-scale CTMs for the Mediterranean Sea.

2 Materials and Methods

In this section the models participating in the intercomparison study are briefly described. More detailed information about the standard setup of models and model internal mechanisms used in the present study can be found in part 1 of this intercomparison study (Fink et al., 2023), which focuses on nitrogen oxides and ozone.

2.1 Models

In this study, five different regional-scale CTM systems run by four institutions participated: CAMx and CHIMERE by AtmoSud, CMAQ by Helmholtz-Zentrum Hereon, EMEP by IVL Swedish Environmental Research Institute and LOTOS-EUROS by TNO Netherlands Organization for Applied Scientific Research. For producing comparable results w.r.t the impact shipping emissions on $PM_{2.5}$ concentrations, the models were set up in a similar way. The same shipping emissions data from STEAM (version 3.3.0.; Jalkanen et al., 2009; Jalkanen et al., 2012; Johansson et al., 2013; Johansson et al., 2017) were used for all CTMs. Land-based emissions (CAMS-REG, v2.0), grid projection (WGS84_lonlat), domain (Mediterranean Sea), grid resolution ($0.1° \times 0.1°$, 12×12 km) and the modeled year (2015) were also consistent (Table 1). The CTM systems were applied in their standard setup for other input data, i.e. the meteorological input data and the boundary and initial conditions differed.

The model domains covered the largest part of the Mediterranean Sea, with a spatial extent ranging in longitude from -0.95° to 29.95° and in latitude from 33.8° to 44.95° (Appendix A). The appointed grid cell size was 12×12 km² interpolated on a $0.1° \times 0.1°$ grid nested in a 36×36 km² grid (except EMEP).

A reference run for present air quality conditions was performed using all models, including all emissions (base case). Furthermore, all models ran once without shipping emissions (noship case). The difference between the estimates with all emissions and the calculations without shipping emissions was then used to calculate the potential impact of ships on pollutant concentrations (zero-out method).

From the results of all models, the annual averaged ensemble mean was calculated based on the daily files. The model run outputs all contained $PM_{2.5}$ in µg/m³ at a daily resolution on a 2D grid from the lowest layer and provided this as a netcdf file following CF conventions. Concentrations in the lowest layer close to ground was used for the intercomparison. The CTM systems calculated $PM_{2.5}$ concentrations in different ways depending on the major physical and chemical mechanisms implemented. Table 1 summarizes the model setups.

The models used in the intercomparison are listed as follows:
- CAMx v6.50 (Ramboll Environ., 2016)
- CHIMERE 2017r4 (Menut et al., 2013)
- CMAQ v5.2 (Byun and Schere, 2006; Appel et al., 2017)
- EMEP MSC-W (Simpson et al., 2012; Simpson et al., 2020)
- LOTOS-EUROS v2.0 (Manders et al., 2017)

Detailed descriptions of the used models can be found in the first part of the intercomparison study (Fink et al., 2023).

165   **Table 1: Main model parameters and input data for the five chemical transport models.**

Model parameter	CAMx	CHIMERE	CMAQ	EMEP	LOTOS-EUROS
Grid resolution inner domain	12x12 km²	12x12 km²	12x12 km²	0.1°x 0.1°	0.1°x 0.1°
Grid resolution outer domain	36x36 km²	36x36 km²	36x36 km²	none	0.5°x 0.25°
Meteorological driver	WPS/WRF	WPS/WRF	COSMO-5 CLM	ECMWF (IFS)	ECWMF (IFS)
Boundary conditions	Mozart-4 output is used and downscaled for time- and space-variable boundary conditions	Gaseous species: LMDz-INCA model (Folberth et al., 2006), with climatology as average monthly fields Aerosols: Global Ozone Chemistry Aerosol Radiation and Transport model GOCART (Ginoux et al., 2001)	IFS_CAMS cycle45r1	provided with the open source model distribution for year 2015; Simple functions for prescribing concentrations in terms of latitude and time-of-year, or time-of-day. (Simpson et al 2012). Boundary conditions of ozone are developed from climatological ozone-sonde datasets as in EMEP Status report 1/2022	CAMS C-IFS global forecast (lateral and top)
Land-based emissions	CAMS-REG v2.2.1	CAMS-REG v2.2.1	CAMS-REG v2.2.1	CAMS-REG v2.2.1	CAMS-REG v2.2.1
Shipping emissions	STEAM v3.3.0	STEAM v3.3.0	STEAM v3.3.0	STEAM v3.3.0	STEAM v3.3.0
Biogenic emissions	MEGAN Model v2.03 output for the year 2015	MEGAN Model v2.04 output for the year 2015	MEGAN Model v3 output for the year 2015	Calculated online: Emissions of isoprene and monoterpenes following Guenther et al. (1993, 1995). Soil NO emissions from soils of seminatural ecosystems are	Calculated online: Emissions of isoprene and monoterpenes following Guenther et al. (1993), using actual meteorological

			specified as a function of the N-deposition and temperature	data. Emission of NO from soil as in Manders-Groot et al. (2016)
Sea salt emissions	Calculation based on Ovadnevaite et al. (2014)	Calculation based on Monahan et al. (1986)	Calculation based on Kelly et al. (2010)	Calculation based on Monahan et al. (1986) and Mårtensson et al. (2003)	Calculation based on Monahan et al. (1986) and Mårtensson et al. (2003)
Dust emissions	Based on approach used in global EMAC (ECHAM/ MESSy; Klingmueller et al., 2017; Astitha et al., 2012).	Calculated online: After parametrization of Marticorena & Bergametti (1995) and Alfaro & Gomes (2001)	Not considered	Key parameter is wind friction velocity. The parameterization after Marticorena & Bergametti (1995), Marticorena et al. (1997), Alfaro & Gomes (2001), Gomes et al. (2003), Zender et al. (2003). Daily emissions from forest and vegetation fires from "Fire INventory from NCAR version 1.0" (Wiedinmyer et al., 2011)	Calculated online: Emissions after Marticorena & Bergametti (1995) with soil moisture as described by Fécan et al (1999). Dust from re-suspension by traffic and agriculture as in Schaap et al. (2009)
Chemical mechanism	CB05	MELCHIOR2	CB05	EmChem 19a	CBM-IV
Aerosol size distribution	PM$_{2.5}$; PM$_{10}$	8 bins: 40 nm to 10 µm	Trimodal size distribution (0.03µm, 0.3µm, 6µm; Binkowski and Roselle, 2003)	PM$_{2.5}$; PM$_{2.5-10}$	PM$_{2.5}$; PM$_{2.5-10}$
Inorganic aerosol module	ISORROPIA (Nenes et al., 1998)	ISORROPIA (Nenes et al., 1998)	ISORROPIA II (Fountoukis and Nenes, 2007)	MARS (Binkowski and Shankar, 1995)	ISORROPIA II (Fountoukis and Nenes, 2007)
Organic aerosol module	SOAP semivolatile scheme (Strader et al., 1999)	Described in Pun et al. (2006)	Updates on SOA as described in Pye et al. (2017)	For SOA the volatility basis set (VBS) approach (Robinson et al.	No organic aerosols in the simulations

				2007; Donahue et al. 2009; Bergström et al. 2012) is used	
Wet deposition scheme	Scavenging model for gases and aerosols (Seinfeld and Pandis, 1998)	The wet deposition in CHIMERE follows the scheme proposed by Loosmore & Cederwall (2004).	Wet deposition is calculated within CMAQ's cloud module as described by Roselle and Binkowsk (1999)	Calculation as described in Emberson et al. (2000); parametrization for different surfaces as in Simpson et al. (2012)	Wet deposition is divided between in-cloud and below-cloud scavenging. The in-cloud scavenging module is based on the approach described in Seinfeld and Pandis (2006) and Banzhaf et al. (2012).
Dry deposition scheme	Resistance model of Zhang et al. (2003)	Dry deposition is as in Wesely (1989)	Dry deposition scheme M3Dry (Pleim, 2001)	As described in Simpson et al. (2012)	Resistance approach following Erisman et al. (1994)

2.1.1 Aerosol Modules

CAMx includes algorithms for inorganic aqueous chemistry (RADM-AQ), inorganic gas-aerosol partitioning (ISORROPIA), and two organic gas-aerosol partitioning and oxidation approaches (VBS or SOAP). Using gas-phase processes, these

170 approaches produce sulfate, nitrate, and condensable organic gases. The hybrid 1.5-D VBS is applied to provide a unified framework for gas-aerosol partitioning and the chemical aging of both primary and secondary atmospheric organic aerosols (Ramboll Environment and Health, 2020). One crucial assumption in PSAT is that PM is allocated to the primary precursor for each type of particulate matter (i.e., PSO_4 is apportioned to SO_x emissions, PNO_3 is apportioned to NO_x emissions, and PNH_4 is apportioned to NH_3 emissions).

175 The full description of CHIMERE's inorganic and organic modules can be found in Menut et al. (2013). CHIMERE's sectional aerosol module includes emitted TPPM, secondary species such as nitrate, sulfate, ammonium, and SOAs. Natural dust and sea salt aerosols can also be produced as passive tracers or interactive species in equilibrium with other ions. Organic matter and elemental carbon can be speciated if an inventory of their emissions is supplied. The utilized models include the aqueous, gaseous, and particulate phases of ammonia, ammonium, nitrate, and sulfate. For instance, in accordance with the ISORROPIA

180 thermodynamic equilibrium model, the model species pNH_3 represents an equivalent ammonium in the particulate phase as the sum of the NH_4^+ ion, NH_3 liquid, NH_4NO_3 solid, and other salts (Nenes et al., 1998).

CMAQ represents aerosol formation and growth using three log-normal distributed modes: the Aitken and accumulation modes are generally less than 2.5 μm in diameter, while the coarse mode contains significant amounts of mass above 2.5 μm. $PM_{2.5}$ and PM_{10} can be obtained from the model-predicted mass concentration and size distribution information.

185   The CMAQ aerosol scheme AERO6 was employed; this scheme expands the chemical speciation of PM by the species Al, Ca, Fe, Si, Ti, Mg, K, and Mn. Sulfuric acid (H_2SO_4), nitric acid (HNO_3), hydrochloric acid (HCl) and ammonia (NH_3) gas phase – aerosol partition equilibrium is solved by the ISORROPIA II mechanism (Fountoukis and Nenes, 2007; Nenes et al., 1998). Contained within this scheme is the formation of SOA from isoprene, terpenes, benzene, toluene, xylene and alkanes (Carlton et al., 2010; Pye and Pouliot, 2012). CMAQ allows for dynamic mass transfer of semi-volatile inorganic gases to

190   coarse mode particles, which facilitates the replacement of chloride by NO_3^- in sea salt aerosols (Foley et al., 2010).

The EMEP MSC-W model version used was rv4.34 with chemical mechanism EmChem 19a (Simpson et al. 2012; Simpson et al. 2020). The mechanism builds on surrogate VOC species (as in Simpson et al. 2012, but extended with benzene and toluene) and has 171 gas-phase and heterogeneous reactions. The model always assumes equilibrium between the gas and aerosol phases using the MARS equilibrium module of Binkowski and Shankar (1995). For SOAs a VBS approach is used

195   (Robinson et al. 2007; Donahue et al. 2009; Bergström et al. 2012). The semivolatile ASOA and BSOA species are considered to oxidize (age) in the atmosphere via OH reactions, whereas all POA emissions are treated as nonvolatile to maintain the emission totals of both the PM and VOC components from the official emission inventories (Simpson et al., 2012). The aerosol module of the EMEP model distinguishes five classes of fine and coarse particles (fine-mode nitrate and ammonium, other fine-mode particles, coarse nitrate, coarse sea-salt, and coarse dust); for dry-deposition purposes, these particles are assigned

200   mass-median diameters (D_p), geometric standard deviations (σ_g), and densities (ρ_p). The aerosol components that are taken into account include sea salt, SO_4^{2-}, NO_3^-, NH_4^+, and anthropogenic main PM. Aerosol water is also considered.

LOTOS-EUROS uses the TNO CBM-IV scheme, which is a modified version of the original CBM-IV scheme (Whitten et al., 1980). N_2O_5 hydrolysis is described explicitly based on the available (wet) aerosol surface area (Schaap et al., 2004). The aqueous phase and heterogeneous formation of sulfate is described by a simple first-order reaction constant (Schaap et al.,

205   2004; Barbu et al., 2009). Aerosol chemistry is represented using ISORROPIA II (Fountoukis and Nenes, 2007).

2.1.2 Wet Deposition Mechanisms

Wet deposition is the predominant removal process for fine particles. The CAMx wet deposition model uses a scavenging method in which the local concentration change rate inside or under a precipitating cloud is determined by a scavenging coefficient. From the top of the precipitation profile to the surface, wet scavenging is estimated for each layer inside a

210   precipitating grid column. The scavenging coefficients of gases and PM are calculated differently depending on the correlations given by Seinfeld and Pandis (2006) (Ramboll Environment and Health, 2020). The wet deposition process in CHIMERE follows the scheme proposed by Loosmore & Cederwall (2004). In CMAQ, wet deposition is calculated in cloud chemistry treatments. The resolved cloud model calculates the contribution of each model layer to the precipitation. Based on a normalized profile of precipitating hydrometeors, CMAQ operates a simple algorithm to assign precipitation amounts to

215　individual layers (Foley et al., 2010). The EMEP model's parameterization of wet deposition processes covers both the in-cloud and sub-cloud scavenging of gases and particles. The parameterization of wet deposition is described in Berge and Jakobsen (1998). There are two types of wet deposition in LOTOS-EUROS: below-cloud scavenging and in-cloud scavenging. The technique is described in Seinfeld and Pandis (2006), and Banzhaf et al. (2012) served as the foundation for the in-cloud scavenging module.

2.2 Emissions

2.2.1 Land-based Emissions

All five models used anthropogenic land-based gridded emissions from the CAMs-REG v2.2 emission inventory for 2015, which is described in Granier et al. (2019) and essentially a further development of the earlier TNO_MACC inventories (Kuenen et al., 2014). A more recent version CAMS-REG-v4.2 is described in detail in Kuenen et al. (2022).

225　For each country, the gridded emission files included GNFR emission sectors for the air pollutants NO_x, SO_2, NMVOC, NH_3, CO, PM_{10}, $PM_{2.5}$, and CH_4. The spatial resolution of the emissions data was $1/10° \times 1/20°$ in longitude and latitude (i.e., ~ 6 × 6 km over central Europe). The CAMS-REG inventory also provides default information to apply the emissions in the CTMs. The height distribution of emissions per GNFR sector was prepared according to Bieser et al. (2011). Based on assignment of PM and NMVOC components at a detailed subsector level, PM and NMVOC speciation profiles are provided for each country, year and GNFR sector. The temporal distribution of emissions is based on the default temporal variation provided along with the CAMS-REG inventory. The NOx splitting was performed according to Manders-Groot et al. (2016).

2.2.2 Shipping Emissions

The shipping emission dataset produced with the STEAM model has a spatial resolution of 12×12 km² and a temporal resolution of one hour. The STEAM v3.3.0 emissions are divided into two vertical layers (0 m to 36 m; 36 m to 1000 m) and are provided for mineral ash, carbon monoxide (CO), carbon dioxide (CO_2), elemental carbon (EC), NO_x, organic carbon (OC), $PM_{2.5}$, particle number count (PNC), sulfate (SO_4), SO_x (containing SO_2 and SO_3) and VOC. To reduce the number of generated emission maps and the computational resources needed to run the STEAM model, VOC emissions were divided into four categories according to their properties as a function of the engine load. Emission factors for VOC are based on the average values taken from various publications (Agrawal et al., 2008; Agrawal et al., 2010; Sippula et al., 2014; Reichle et al., 2015).

240　All shipping emissions are included in the lowest layer of CAMx. In CAMx, all gridded emissions are at the ground level except punctual and linear emissions. For CHIMERE, 88 % of the emissions below 36 m and all shipping emissions above 36 m were added to the second layer. Only 12 % of the emissions below 36 m were allocated to the model's lowest layer. The STEAM emission dataset, which included stack heights, was used for this procedure. In CMAQ, shipping emissions were split between the two lowest levels; those below 36 m were ascribed to the lowest layer, while those above 36 m were positioned in the second layer. The height of the lowest and of the second layer in CMAQ are 42 m for each. The STEAM emissions were

summed from hourly to daily emissions and attributed to the lowest layer (up to 90 m) in the EMEP simulations. In LOTOS-EUROS, emissions below 36 m were divided into two layers: the first layer was 25 m thick (~ 70 % of emissions), and the second layer was 30 m thick (~ 30 % of emissions). Over 36 m, emissions are separated into various height groups: 30 % were between 36 m and 90 m, 30% were between 170 m and 90 m, 30 % were between 170 m and 310 m, and 10 % were between 310 m and 470 m. These emissions were placed in the second or third model layers because of the dynamic second model layer, which follows the meteorological boundary layer. All emissions were placed in this second layer when the meteorological boundary layer was well mixed and vertically extended (higher than 470 m), while some emissions were placed in the third layer when the boundary layer was shallow.

2.3 Observational Data, Statistical Analysis and Analysis of Model Results

The model findings regarding the total surface $PM_{2.5}$ concentrations from the five CTM systems were compared to data from the air quality monitoring network obtained from the EEA download service (https://discomap.eea.europa.eu/map/fme/AirQualityExport.htm, 2021). The locations of the measurement stations are shown in Figure A1, and full information on the stations can be found in Appendix B.

The stations were chosen based on the following criteria: i) the station type was "background," ii) the station elevation was less than 1000 meters, and iii) the station recorded data for more than one of the following pollutants: NO_2, O_3, or $PM_{2.5}$. In the first part of this intercomparison study (Fink et al., 2023), NO_2 and O_3, were discussed. Since simulating the potential impact of ships was the main focus of this study, stations near the sea were preferably chosen.

The model findings regarding the total surface $PM_{2.5}$ concentrations from the five CTM systems were compared to existing observations. The RMSE, NMB, and correlation coefficient R were determined for each monitoring station to quantify the model performance, as described in the previous study (Fink et al., 2023).

A categorization scheme for the correlations was established as described in Schober et al. (2018), with weak (0.00-0.39), moderate (0.40-0.69) and strong (0.70-1.00) correlations.

To compare the predicted daily mean concentrations to the measurements recorded at representative sites, time series were employed. In addition, based on hourly data, the yearly mean potential ship impact was determined. Boxplots based on yearly values obtained from hourly data at each station were used to graphically compare the model performances using the R, NMB, and RMSE metrics. Annual mean values based on hourly data were utilized for the intercomparison maps. Based on hourly data, the correlations between models were determined for each grid cell.

3 Results

3.1 PM$_{2.5}$ Model Performance

275   Regarding the model performance, time series can give an overview of the performance throughout the whole year. Figure 1 displays the average values at all 28 measurement stations. CAMx, CMAQ, EMEP and LOTOS-EUROS underestimate the actual measured data. The largest underestimations are found for CMAQ (NMB = -0.42) and LOTOS-EUROS (NMB = -0.54). Contrary to the other CTM systems, CMAQ does not consider dust contribution, which can cause underestimations in PM$_{2.5}$. However, the correlations between the modeled and measured data is strongest for these models (CMAQ: R = 0.50, LOTOS-

280   EUROS: R = 0.54; Table 2). No correlation can be found between the measured and modeled data for CHIMERE (R = 0.02), on the other hand CHIMERE displays only a slight overestimation of the actual data (NMB = 0.06). The simulated potential impacts of ships at all measurement stations are between 5.7 % (CMAQ) and 13.8 % (CAMx; Table 2) as annual average. The simulated ship impacts on PM$_{2.5}$ concentration are within the ranges stated in other studies. In a review of studies regarding the impact of shipping emissions on coastal regions, Viana et al. (2014) reported PM$_{2.5}$ impacts of shipping between 5 % and

285   14 %. Aksoyoglu et al. (2016) found PM$_{2.5}$ concentrations between 10 % and 15 % along coastal areas due to ship traffic. Ship impacts of approximately 20 % in the southern coastal region of the Iberian Peninsula were found by Nunes et al. (2020). Although in this study, the utilized models underestimated the actual measured total PM$_{2.5}$ concentrations, they slightly overestimated the relative potential ship impact on PM$_{2.5}$ compared to previous measurement studies. Donateo et al. (2014) measured a proportion of 7.4 % of ships to total PM$_{2.5}$; Pandolfi et al. (2011) measured a proportion of shipping in the bay of

290   Algeciras to PM$_{2.5}$ concentrations between 5 % and 10 %. Argawal et al. (2009) monitored PM$_{2.5}$ at the harbor of Los Angeles and found PM$_{2.5}$ contributions from ships up to 8.8 %. Predominating secondary particles in PM$_{2.5}$ for potential ship impact in the present study can explain the deviations to the measurement studies.

The RMSE is very similar for all models with a value between 10.7 µg/m³ and 12.2 µg/m³. However, the RMSE is strongly determined by high concentrations and can be biased by outliers. This might explain the similar RMSE derived from

295   CHIMERE despite the lack of correlation. The mean RMSE from different models for PM$_{2.5}$ in Europe found in the AQMEII intercomparison study by Im et al. (2015) was 6.19 for rural stations and 10.26 for urban stations and is similar as the RMSE calculated in the present study.

The underestimation of PM$_{2.5}$ concentrations by four out of five models is consistent with results by Im et al. (2015) who reported an underestimation of particulate matter for all participating models, with largest underestimations observed in the

300   Mediterranean region. They stated that the representation of dust and sea-salt emissions had a large impact on the simulated PM concentrations and that uncertainties remain when trying to identify the reasons for the model bias (Im et al., 2015). Additionally, in a study by Gašparac et al. (2020), underestimations were also found when using EMEP and WRF-Chem to model PM$_{2.5}$ at rural stations in Europe. Solazzo et al. (2012) performed an operational model evaluation for ten models and found that the models underestimated the monthly mean PM$_{2.5}$ surface concentrations in Europe in most cases.

305

Table 2: Correlation (R), normalized mean bias (NMB), root mean square error (RMSE), observational (obs) and modeled (mod) mean PM$_{2.5}$ values for 2015 over all 28 stations. Observed mean value for all stations is 14.6 μg/m³.

	Correlation	NMB	RMSE (μg/m³)	Mod (μg/m³)	Absolute potential ship impact (annual mean average at all stations) in μg/m³	Relative potential ship impact (annual mean average at all stations) in %
CAMx	0.19	-0.33	11.5	8.9	1.2	13.8
CHIMERE	0.02	0.06	11.1	14.3	1.8	13.2
CMAQ	0.50	-0.42	10.7	8.3	0.5	5.7
EMEP	0.17	-0.33	12.2	8.9	0.9	9.1
LOTOS-EUROS	0.54	-0.53	10.9	6.8	0.6	9.5
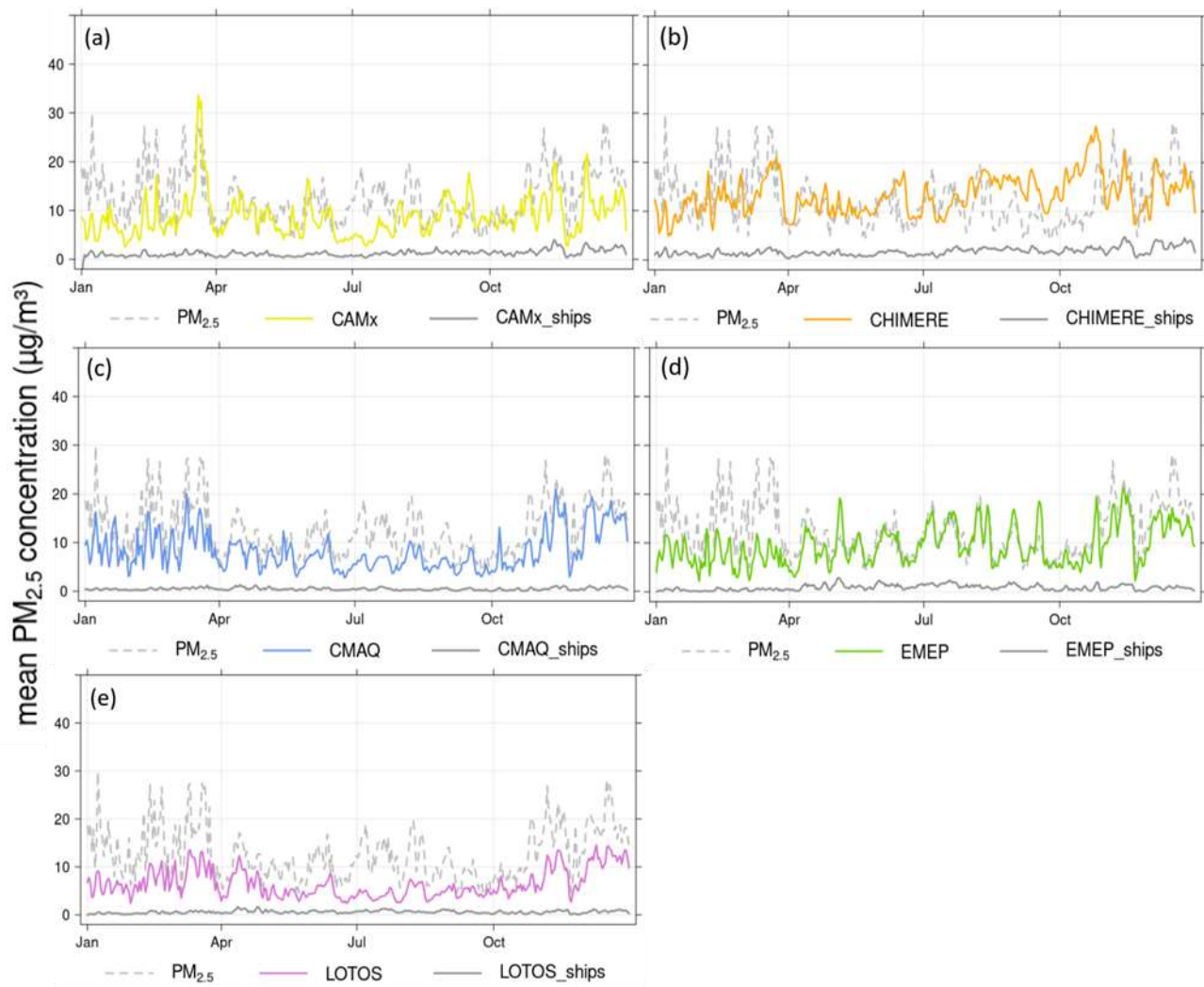
Figure 1: Time series with daily mean PM$_{2.5}$ concentration in 2015, averaged for all stations and the respective grid cells of the models. (a) = CAMx, (b) = CHIMERE, (c) = CMAQ, (d) = EMEP, (e) = LOTOS-EUROS. Dashed gray line = measured data, colored lines = modelled data, gray line = modelled potential ship impact.

3.2 PM$_{2.5}$ Spatial Distribution

The highest PM$_{2.5}$ values are simulated by all five models in northern Italy, the Balkan Peninsula and northern Africa (Figure 2). The PM$_{2.5}$ annual mean concentration results show that CHIMERE has the highest annual mean values of 13 µg/m³ to 15 µg/m³ for the eastern part of the domain and over water, whereas LOTOS-EUROS displays the lowest values with 2.0 µg/m³ to 4.0 µg/m³ in most regions (Figure 2). CMAQ, CAMx and EMEP show similar model PM$_{2.5}$ outputs with diverse values distributed between 2.0 µg/m³ and 11 µg/m³ over the domain. The ensemble mean value over the whole domain is 8.6 µg/m³ (Figure 8 a). All five models display high PM$_{2.5}$ concentrations of >15 µg/m³ in the Po valley. In this area, Kiesewetter et al. (2015) and Clappier et al. (2021) also simulated high values between 20 µg/m³ and 45 µg/m³ for 2015. As demonstrated in Table 3, the correlation between the base-run model results with all emissions is strongest between EMEP and CMAQ (R = 0.59) and CAMx and CMAQ (R = 0.42). In Fink et al. (2023) a high correlation was found between CAMx and CHIMERE simulated NO$_2$ and O$_3$ concentration because both models used the same meteorology. Nevertheless, the present study reveals that particle chemistry causes more differing results due to a higher complexity in the calculations.

The potential impacts of PM$_{2.5}$ from ships simulated by CAMx, LOTOS-EUROS and EMEP have the largest areas with values up to 25 % at the main shipping routes (Figure 3). CMAQ and CHIMERE have a potential shipping impact of 15 % along the main shipping lines close to the African coast. This impact is lower than that shown in other studies. Aksoyoglu et al. (2016) found the highest impacts of 25 % to 50 % of total PM$_{2.5}$ concentrations when using CAMx along main shipping routes. Sotiropoulou & Tagaris (2017) used CMAQ for simulations and stated that emissions from shipping are likely to increase PM$_{2.5}$ concentrations during winter by up to 40 % over the Mediterranean Sea, while during summer, they simulated an increase of more than 50 %. In both studies, the modeled year is 2006, which might explain the deviation to the present study using a different year. Regarding coastal areas in the present study, potential shipping impacts reaching to 12 % to 15 % are simulated. Regarding the absolute potential impacts of ships at the main shipping routes, CAMx, CHIMERE and EMEP show values of 2.0 µg/m³, and the values simulated by CMAQ and LOTOS-EUROS are between 0.5 µg/m³ and 1.0 µg/m³ (Figure 4). The median of the ensemble mean is 0.85 µg/m³ (Figure 4 and 8). Aksoyoglu et al. (2016) simulated similar shipping impacts with CAMx, with values mainly between 0.5 µg/m³ and 1.0 µg/m³.

The sea salt concentrations might partly give an explanation for the differing PM$_{2.5}$ concentration distribution among the models. The annual mean sea salt (NaCl) concentration in fine and coarse showed the highest values for CHIMERE, which might be an explanation for the high PM$_{2.5}$ absolute concentration (Figure S1). The LOTOS-EUROS sea salt displayed lowest concentrations, also the overall PM$_{2.5}$ concentration is lowest compared to the other CTMs. The sea salt concentration was highest (up to 7.0 µg/m³) over sea in areas with high surface wind speed for CHIMERE, CMAQ, EMEP and LOTOS-EUROS (Figure S2). This can be confirmed by the correlation for wind speed and sea salt at several points over water for CMAQ, EMEP and LOTOS-EUROS (Figure S3; Table S4). CAMx is excluded from the analysis since sea salt is only present in fine PM.

Solazzo et al. (2012) demonstrated that the chemical components SO_4^{2-}, NO_3^- and NH_4^+ were better reproduced by nine CTMs than total $PM_{2.5}$. They concluded from this result that other components (e.g., organic aerosols) could be simulated with less accuracy than inorganic components.

350

Table 3: Correlations between models for the $PM_{2.5}$ base runs of the whole domain (all grid cells), based on daily $PM_{2.5}$ total concentration data.

All	CAMx	CHIMERE	CMAQ	EMEP	LOTOS-EUROS
LOTOS-EUROS	0.07	0.00	0.26	0.06	-
EMEP	0.32	0.17	0.59	-	
CMAQ	0.42	0.19	-		
CHIMERE	0.40	-			
CAMx	-				
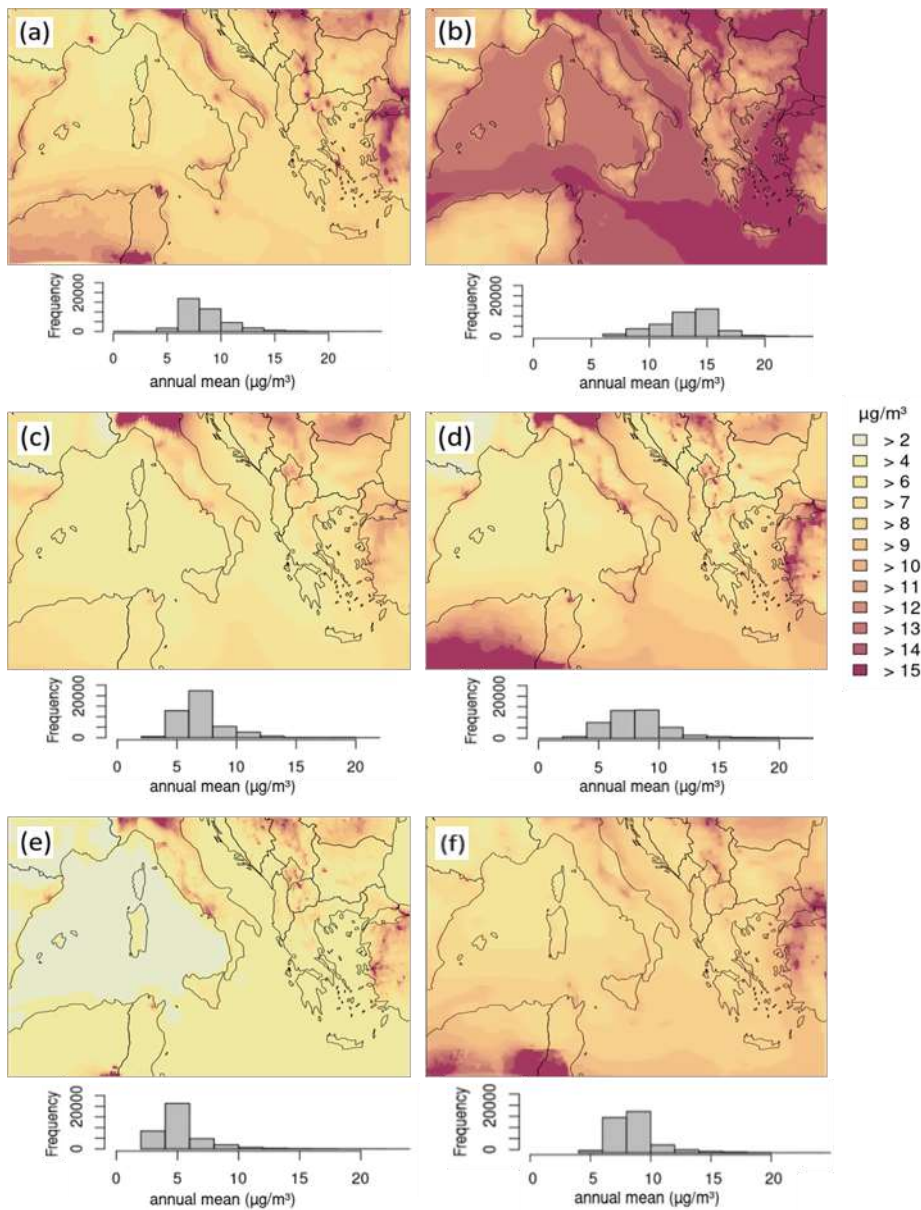
Figure 2: Annual mean PM$_{2.5}$ total concentration. (a) = CAMx, (b) = CHIMERE, (c) = CMAQ, (d) = EMEP, (e) = LOTOS-EUROS, (f) = ensemble model mean. Below the domain figure is the respective frequency distribution displayed for the annual mean PM$_{2.5}$ concentration, referred to the whole model domain.
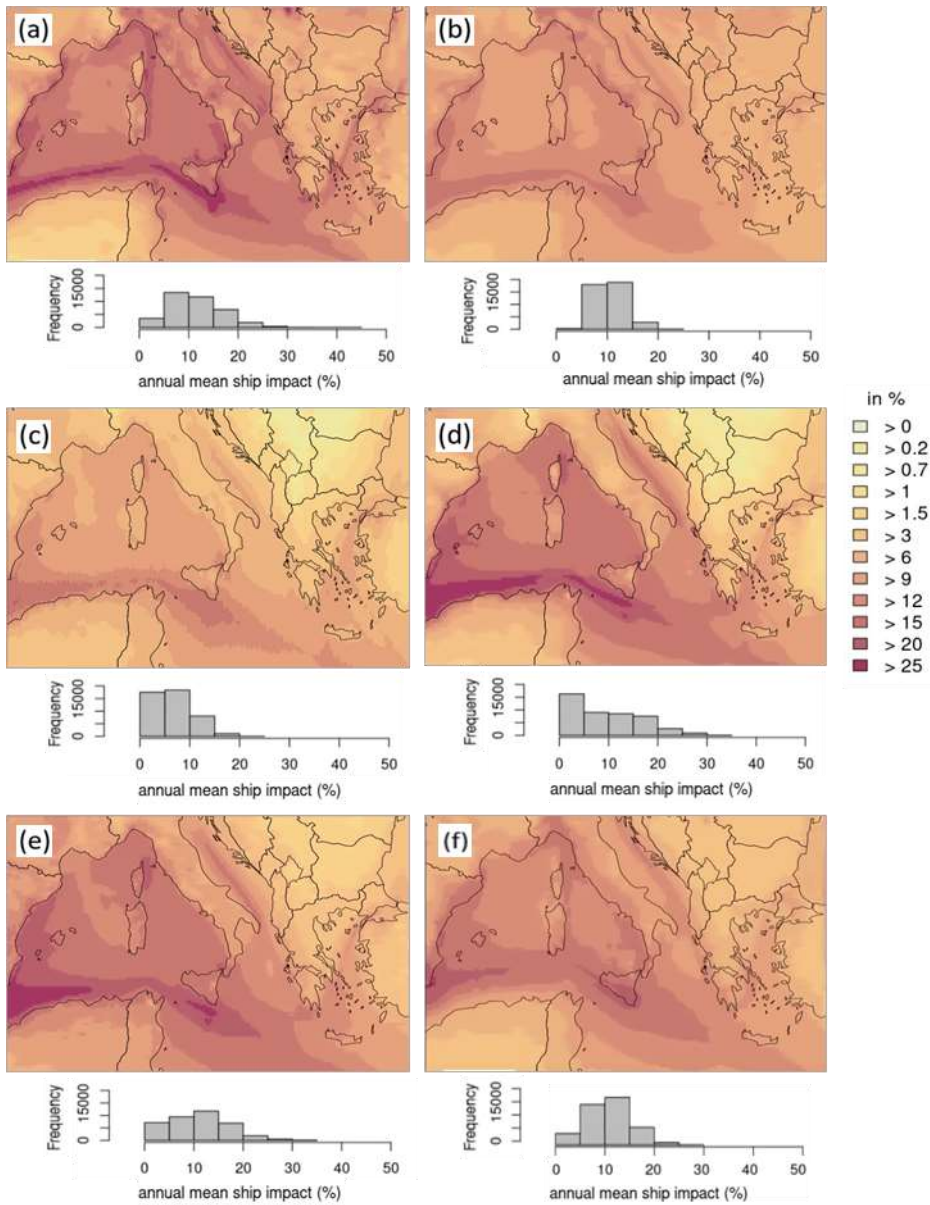
Figure 3: Annual mean PM$_{2.5}$ relative potential ship impact. (a) = CAMx, (b) = CHIMERE, (c) = CMAQ, (d) = EMEP, (e) = LOTOS-EUROS, (f) = ensemble model mean. Below the domain figure is the respective frequency distribution displayed for the annual mean PM$_{2.5}$ potential ship impact, referred to the whole model domain.

360
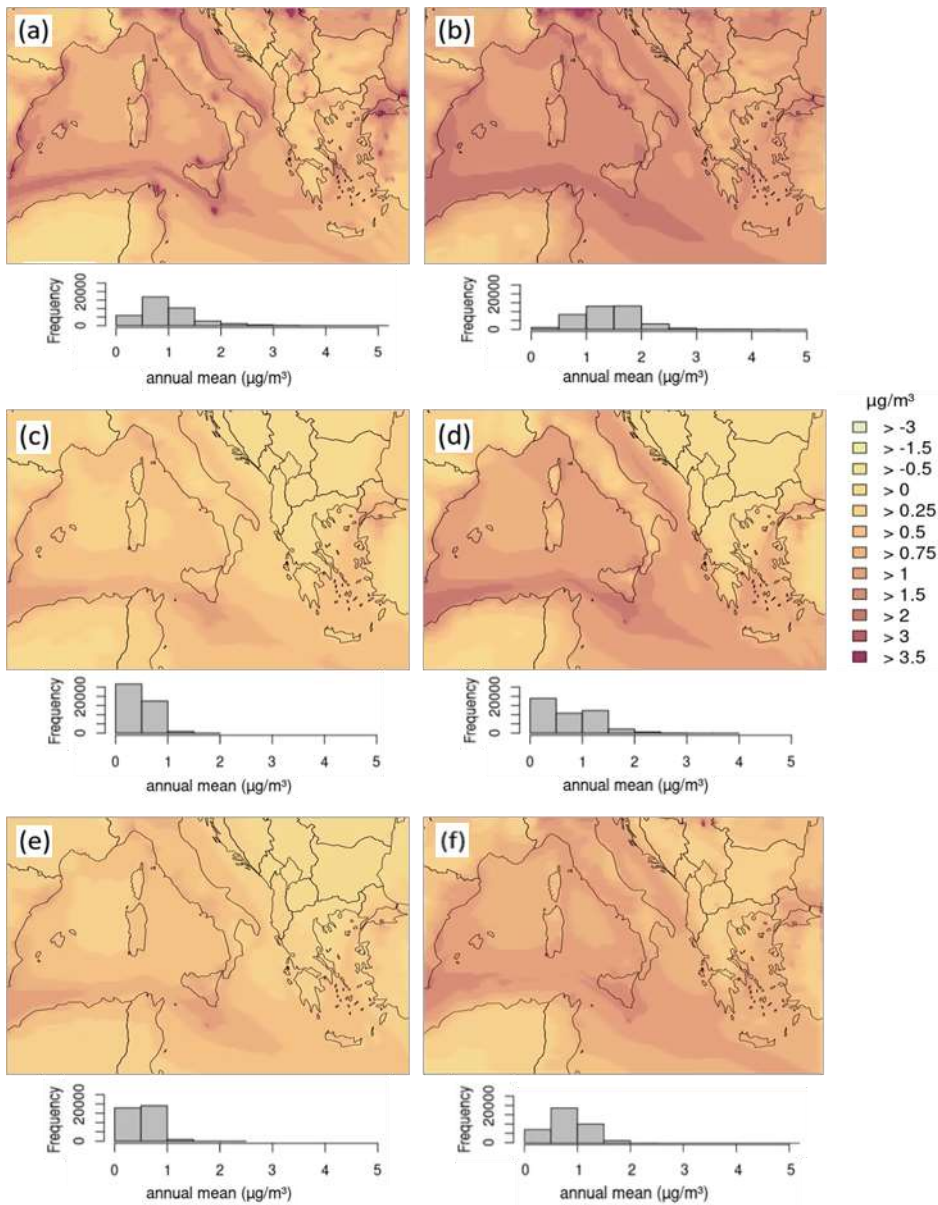
Figure 4: Annual mean PM$_{2.5}$ absolute potential ship impact. (a) = CAMx, (b) = CHIMERE, (c) = CMAQ, (d) = EMEP, (e) = LOTOS-EUROS, (f) = ensemble model mean. Below the domain figure is the respective frequency distribution displayed for the annual mean PM$_{2.5}$ potential ship impact, referred to the whole model domain.

3.3 Precursors

High amounts of NH_3, HNO_3, SO_2 and NO_2 are expected to lead to higher values of the aerosol particles composed of NH_4^+, NO_3^- and SO_4^{2-}. The modelled spatial distributions of these precursors can be found in the Supplements (HNO_3: Figures S5-S7; NH_3: Figures S9-S11; SO_2: Figures S12-S14; and NO_x: Figures S15-S17).

365   The highest annual mean HNO_3 concentration among the base runs is found in the CAMx and the CHIMERE simulations over water (2.0 µg/m³ to 5.0 µg/m³); over land, the values are between 0.0 µg/m³ and 1.5 µg/m³, and those in coastal areas reached 2.0 µg/m³ (Figure S5). The absolute potential ship impact is also highest in CAMx and CHIMERE at the main shipping routes and over water areas (1.0 µg/m³ to 3.0 µg/m³). The relative potential ship impact on total HNO_3 ranges from 60 % to 85 % along the main shipping routes simulated by CAMx, CMAQ and EMEP (Figure S5). These impacts are slightly lower for

370   CHIMERE and LOTOS-EUROS (60 % to 75 %).

The high HNO_3 concentrations simulated by CAMx and CHIMERE might be traced back to the NO_2 concentrations; these two models also show higher NO_2 concentrations than the other CTMs (Figure S15; Fink et al., 2023). This can be explained by the fact that HNO_3 is a major NO_2 sink, especially during daytime. NO_2 is primarily emitted from anthropogenic fossil fuel burning but also comes from natural sources (i.e., soil emissions, biomass burning, lightning). During daytime, the main NO_2

375   removal mechanism is oxidation by hydroxyl (OH) radicals to form HNO_3 (Seinfeld and Pandis, 1998). It can be concluded that in areas with shipping, more NO_2 enters the atmosphere, the total NO_2 concentration increases, and as a result of the subsequent reactions, the HNO_3 concentration also increases. The HNO_3:NO_2 ratio can be used to normalize the data (Figure S8). The ratio displays low values over land and along main shipping routes, indicating that in these areas, both the HNO_3 and NO_2 concentrations are high. Low HNO_3:NO_2 ratio could also mean that only a small amount of OH is present,

380   especially in areas with low O_3 concentration.

After its formation, HNO_3 can react with NH_3 to be neutralized and form particles when NH_3 is in excess. The annual mean NH_3 for the base case show very similar patterns and values among all models (Figure S9). The highest concentrations of NH_3 with all emission sources are located over land areas with values up to 2.5 µg/m³, which can be traced back to agriculture, the main source of NH_3 emissions (Behera et al., 2013). Over water areas, the NH_3 concentration is very small, typically between

385   0.0 µg/m³ and 0.3 µg/m³, except for the slightly higher results modeled by LOTOS-EUROS, with values between 0.2 µg/m³ and 0.8 µg/m³. Negative potential ship impacts (-0.01 µg/m³ to -1.0 µg/m³ and -2.5 % to -150 %; Figure S10 and S11) are found for the whole domain in all five models. The relative ship impacts are lowest at the main shipping routes for CAMx and EMEP. The spatial distribution of the NH_3 relative ship impact is opposite to the simulated HNO_3 values; at the main shipping routes with low NH_3 and high HNO_3 values. These results indicate that available NH_3 reacts directly with HNO_3 to form

390   particles (i.e., NH_4NO_3). Thus, NO_x emissions from shipping lead to HNO_3 formations and subsequent NH_3 consumption, e.g. shipping impacts on NH_3 concentrations are usually negative.

The CAMx simulations show highest SO_2 concentrations with more than 10 µg/m³ in some areas in Western Turkey, in urban areas and along major shipping lanes (Figure S12). The results from the other four CTMs display high values around the

Bosporus and in some areas over the Balkan Peninsula with values of 11 µg/m³ and much lower concentrations along the main shipping routes. The potential ship impacts are similarly high in CAMx and CHIMERE (1.0 µg/m³; 85 % to total concentration; Figure S13 and S14), with the highest values along the major shipping route north of the African coast. The CMAQ, EMEP and LOTOS-EUROS results display similarly high values but only in small areas. The modeled year is 2015, so the global 0.5 % sulfur cap of marine fuels was not yet effective. Heavy fuel oils with sulfur contents reaching 3.50 % were used until 2020 to power ships; thus, the SO_2 emitted from ships in the present study is still high and it can be expected that it has a large impact on secondary particle formation.

3.4 Inorganic Aerosol Species

3.4.1 Concentrations

In the Northern Hemisphere, secondary inorganic ammonium, sulfate and nitrate aerosols represent a large fraction of the $PM_{2.5}$ composition (Jimenez et al., 2009). Ammonium preferentially binds to SO_4^{2-} in atmospheric aerosols in the form of $(NH_4)_2SO_4$. NH_4NO_3, on the other hand, is formed in areas characterized by high NH_3 and HNO_3 conditions and low H_2SO_4 conditions. The results of the CTMs with regard to these three particle species and their potential ship impacts are considered in the following section. The spatial distributions of the total concentrations and absolute potential ship impacts of the individual species can be found in the supplements (NH_4^+: Figures S18 & S19; SO_4^{2-}: Figures S20 & S21; and NO_3^-: Figures S22 & S23), spatial distribution of relative potential ship impact is shown in Fig. 5 to Fig. 7.

The spatial distribution of NH_4^+ shows that the lowest total annual mean can be found mainly in the southwestern part of the domain (approximately 0.0 µg/m³) and the highest in the Po Valley and Bosporus (1.5 µg/m³, Figure S18). The relative ship impacts are very similar for all models (0.25 % to 5.0 % over land, 10 % to 25 % over water; Figure 5) as well as for the absolute ship impact (Figure S16). Aksoyoglu et al. (2016) simulated NH_4^+ values between 0.0 µg/m³ and 0.2 µg/m³ in the Mediterranean region, with higher concentrations (0.4 µg/m³) in the Po valley. This is within the same range of concentrations in the present study. Ge et al. (2021) used the EMEP model to simulate global particle species concentrations and compared them to measured concentrations. They showed in their study that the NH_4^+ concentrations simulated in Europe in 2015 were overestimated by factor 2 compared to the actual measured NH_4^+ concentrations. The measurements displayed a mean of 0.45 µg/m³. The ensemble mean for NH_4^+ in the present study (0.6 µg/m³, Figure 8 a) is in good agreement with these measurements. However, a previous study on measured compared with simulated aerosol distribution with the CMAQ model displayed a slight underestimation of NH_4^+ (Matthias, 2008).

The NH_4^+ proportion to total $PM_{2.5}$ is similar among all models (5.6 % to 7.8 %; Figure 8 a, Table 4), and only LOTOS-EUROS displayed a relatively high share (12.2 %). This pattern is similar for the ship impacts, where all models show proportions between 9.1 % and 12.6 %, but higher values are simulated by LOTOS-EUROS (23.5 %; Figure 8 b, Table 5).

SO_4^{2-} is the oxidation product of SO_2, which is primarily emitted by anthropogenic processes such as fossil fuel combustion, petroleum refining, and metal smelting (Zhong et al., 2020). In the present study, SO_4^{2-} is the main contributor to total $PM_{2.5}$

mass (Figure 8, Table 4). Especially in the model ensemble mean for the absolute ship-related concentrations, SO_4^{2-} makes up 44.6 % of $PM_{2.5}$ (Figure 8 b, Table 5). The annual mean SO_4^{2-} total concentration is highest for CHIMERE in the eastern part of the domain, reaching 6.0 µg/m². EMEP displays a SO_4^{2-} concentration within the ranges of the other models CAMx, CMAQ and LOTOS-EUROS in the western part of the domain. These models show very similar spatial distributions with
430　concentrations up to 2.0 µg/m³. The median ensemble mean for the run with all emission sources is 2.0 µg/m³. This ensemble mean is low in comparison with the results of Solazzo et al. (2012); they found a mean value of 6.0 µg/m³ but considered a larger European area that included the areas with highest SO_4^{2-} concentrations in Europe. For this larger area, Solazzo et al. (2012) found that the used models underestimated SO_4^{2-} by 7 % to 17 %.

In the present study, the relative potential ship impact on total SO_4^{2-} is lowest over land, with 0 % to 3.0 %, and higher in
435　coastal areas, with values from 6 % to 20 % (Figure 6). Along the main shipping routes it is highest, reaching 50 % for CAMx, EMEP and LOTOS; for CHIMERE and CMAQ, it is lower with values reaching 30 %. Aksoyoglu et al. (2016) showed similar relative potential ship impacts of 50 % to 60 % in the western Mediterranean. In their study, values were between 0.0 µg/m³ to 1.0 µg/m³ over land areas, but over water along the main shipping routes they were highest at 2.2 µg/m³.

Mallet et al. (2019) traced back higher SO_4^{2-} in the eastern part of the domain due to westerly winds. In the present study, we
440　found this higher concentration for SO_4^{2-} in the eastern part of the Mediterranean as well. On Lampedusa, they found ammonium sulfate contributed 63 % to PM_1 mass, followed by organics (Mallet et al., 2019). In our study, the organics/others had highest share on total $PM_{2.5}$ when considering all emission sources, followed by sulfate and ammonium. In the present study, CTM systems simulated lower values for ship impacts; over land, they are 0.0 µg/m³ to 0.03 µg/m³, and along the main shipping routes, they reached 0.9 µg/m³. Regarding the absolute ship impacts on SO_4^{2-}, the model simulations
445　displayed similar concentrations and are slightly lower for CMAQ and LOTOS-EUROS (Figure S21) compared to the other models. Especially over water areas, large areas with considerable SO_2 and SO_4^{2-} concentrations can be seen. Because NH_4^+ is preferably bound to SO_4^{2-} in atmospheric aerosols to form $(NH_4)_2SO_4$, in areas over water, less NH_4NO_3 forms.

Im et al. (2014) suggested in their intercomparison study that over Europe, SO_4^{2-} levels were underestimated by most models; only a few models overestimated SO_4^{2-} concentrations in Europe. The underestimating models were WRF-CHEM models, and
450　the SO_4^{2-} underestimations were attributed to the absence of SO_2 oxidation in cloud water in the heterogeneous phase.

The highest annual mean NO_3^- total concentrations is simulated over land areas especially over Italy and in the Balkan states (> 2 µg/m³; Figure S19), lowest concentration are over sea. CAMx, CMAQ and LOTOS-EUROS show higher concentrations compared to results derived from CHIMERE. The concentrations over water are lower than those over land. The ensemble median of all CTMs over the whole domain is 0.63 µg/m³ (median value; Figure 8 a). The absolute potential impacts of ships
455　on the total NO_3^- concentrations are similar among all models, displaying values mainly between -0.005 µg/m³ and 0.15 µg/m³; only CMAQ demonstrates relatively low values along the main shipping routes (-0.5 µg/m³), and CAMx has higher values (1.0 µg/m³) in some coastal areas (Figure S20). This can be explained by higher SO_4^{2-} concentrations derived from SO_2 emissions. Sulfate replaces nitrate as long as ammonia concentration is low. In model simulations with ships, NO_3^- can decrease because ammonia is already taken from sulfur emissions from ships. Aksoyoglu et al. (2016) found similar results for the

460   Mediterranean Sea considering the NO_3^- concentrations, with values between 0.0 µg/m³ and 0.2 µg/m³. Im et al. (2014) showed that simulated NO_3^- levels were overestimated by most of the CTMs by more than 75 %. Higher concentration over water than over land due to NH_4NO_3 formation are found in areas characterized by high NH_3 and HNO_3 conditions and low H_2SO_4 conditions. In the present study, the relative potential ship impacts on NO_3^- displays contradicting tendencies among the models (Figure 7). The CAMx, EMEP and LOTOS model results are similar, with relative potential ship impacts over land of 0.0 %

465   to 5.0 % (in the Balkan states), those in coastal areas and Italy of 10 % to 25 % and those along main shipping routes of 50 % to 65 % or even up to 85 %. CHIMERE and CMAQ display lower relative potential ship impacts. For CMAQ, the impact is even negative along the main shipping routes, at -25 %. Sulfur dioxide or ammonia, might lead to negative NO_3^- impact, because the NO_2 emissions from ships would make a positive contribution to nitrate formation. Therefore, without ships, a $(NH_4)_2SO_4$ should be formed, which is more stable than NH_4NO_3. These low values in the aerosol species for CMAQ but

470   higher values for EMEP, CAMx and LOTOS represented the $PM_{2.5}$ ship impacts and might partly explain the deviations in $PM_{2.5}$. Furthermore, in CMAQ the coarse mode in nitrate and ammonium has a larger share compared to the other CTMs. A more detailed discussion will be given in Sect. 4.

Regarding the $PM_{2.5}$ composition, the share of other particles, which contain mainly organics but also e.g. sea salt, is highest compared to the inorganic species (Figure 8). Nevertheless, the particle composition revealed varying distributions in the ship-

475   related $PM_{2.5}$ concentration. Here, inorganic particle species have relatively high percentages compared to organic aerosols. In some cases, sulfate has an even higher share of the total $PM_{2.5}$ than other particles.

The seasonal variability in particle species shows that NO_3^- is more temperature-dependent than SO_4^{2-} and NH_4^+. NO_3^- is higher in winter and spring but lower in summer and autumn. This pattern can be found in all CTM simulations. For $PM_{2.5}$, on the other hand, no discernible pattern is found regarding seasonal variability. In particular, the ensemble mean $PM_{2.5}$ concentration

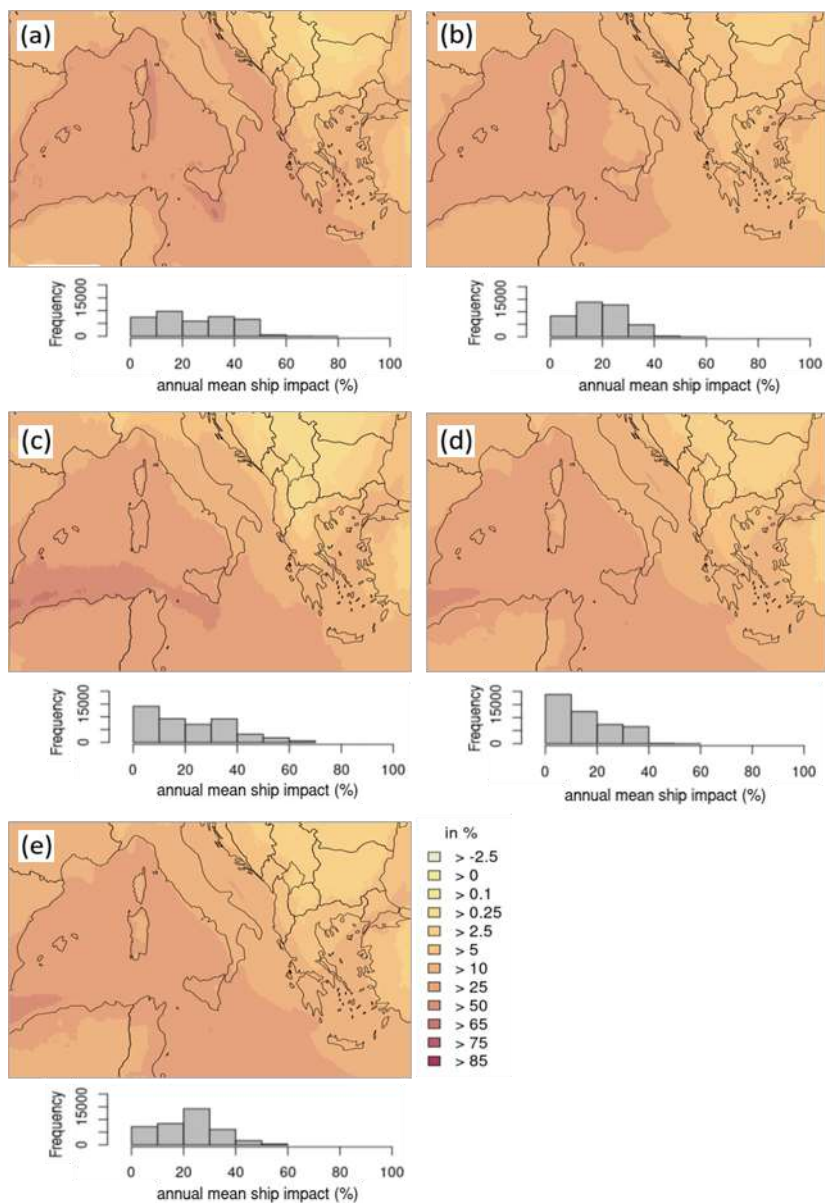480   remained within the same range in all seasons.

Figure 5: Annual mean NH$_4^+$ relative potential ship impact. (a) = CAMx, (b) = CHIMERE, (c) = CMAQ, (d) = EMEP, (e) = LOTOS-EUROS. Below the domain figure is the respective frequency distribution displayed for the annual mean NH$_4^+$ potential ship impact, referred to the whole model domain.
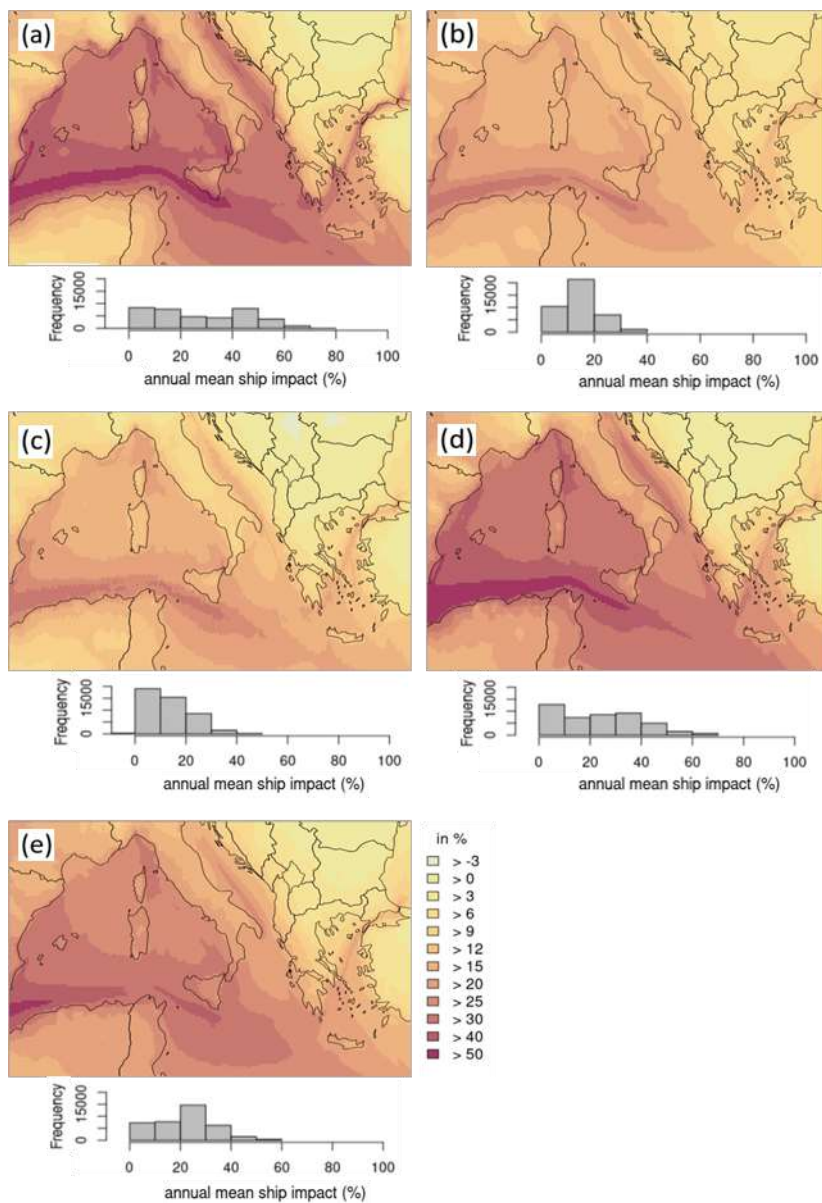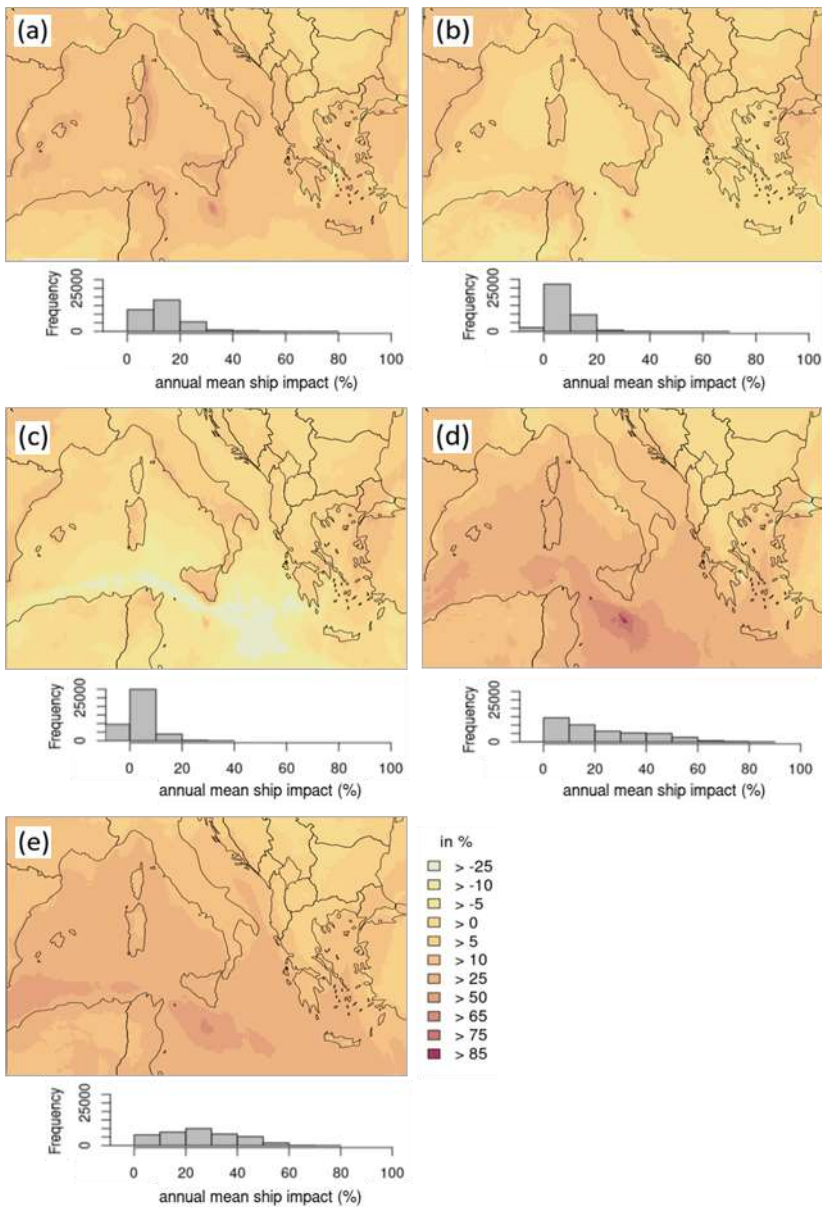
Figure 6: Annual mean SO₄²⁻ relative potential ship impact. (a) = CAMx, (b) = CHIMERE, (c) = CMAQ, (d) = EMEP, (e) = LOTOS-EUROS. Below the domain figure is the respective frequency distribution displayed for the annual mean SO₄²⁻ potential ship impact, referred to the whole model domain.
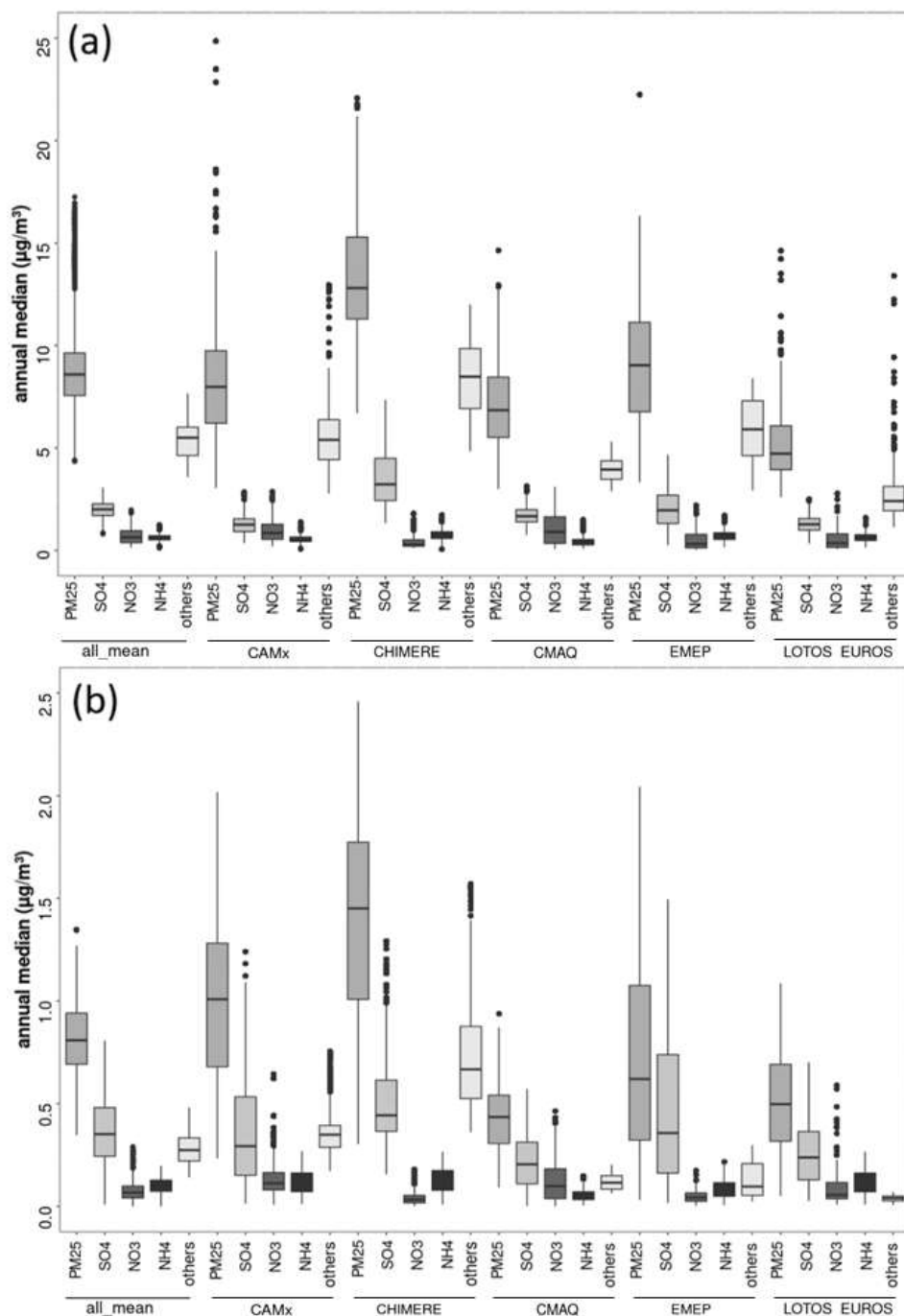
Figure 7: Annual mean NO₃ relative potential ship impact. (a) = CAMx, (b) = CHIMERE, (c) = CMAQ, (d) = EMEP, (e) = LOTOS-EUROS. Below the domain figure is the respective frequency distribution displayed for the annual mean NO₃ potential ship impact, referred to the whole model domain.

26

Figure 8: (a) Boxplots for concentrations of PM$_{2.5}$, and the PM2.5 components SO$_4^{2-}$, NO$_3$, NH$_4^+$ and "others" as simulated by the five CTMs. The ensemble mean is "all_mean". Others is calculated as PM$_{2.5}$ minus the sum of SO$_4^{2-}$, NO$_3$ and NH$_4^+$. Data is based on the whole domain (all grid cells) and hourly data for all emission sources ("emisbase"). (b) Same as (a) but for ships only.

Table 4: Relative particle species of total PM$_{2.5}$ emissions.

	Ensemble mean	CAMx	CHIMERE	CMAQ	EMEP	LOTOS-EUROS
SO$_4^{2-}$	22.8	14.6	27.0	23.8	22.5	24.8
NO$_3$	8.0	11.1	3.1	14.5	5.6	10.6
NH$_4^+$	7.1	6.5	5.6	6.2	7.8	12.2
Other	62.1	67.8	64.3	55.5	64.1	52.4

490 **Table 5: Relative particle species of total shipping-related PM$_{2.5}$.**

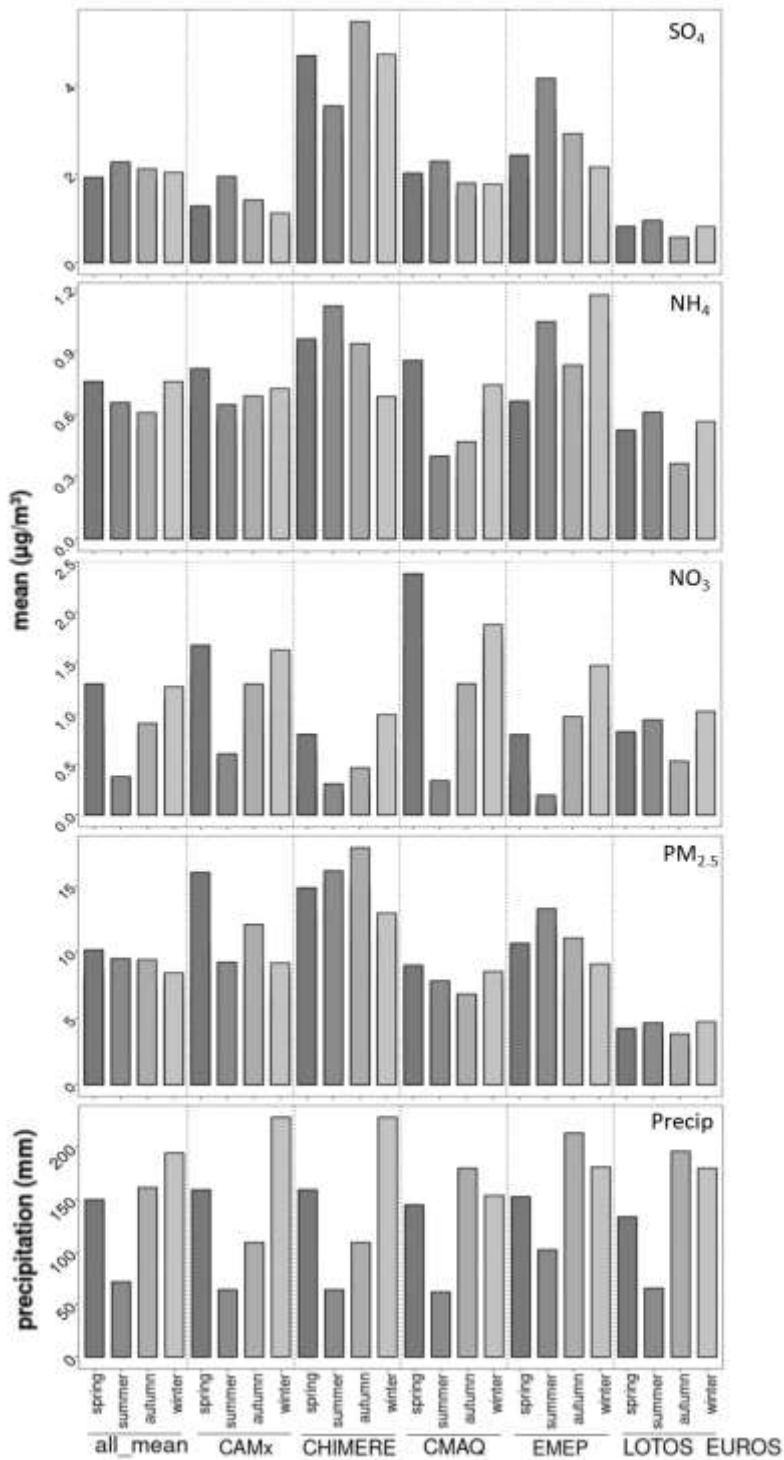|	Ensemble mean	CAMx	CHIMERE	CMAQ	EMEP	LOTOS-EUROS
SO$_4^{2-}$	44.6	37.0	36.0	48.5	63.9	51.8
NO$_3$	8.6	13.1	2.5	11.9	6.6	16.9
NH$_4^+$	12.4	11.7	9.1	12.6	11.8	23.5
Other	24.4	38.2	52.4	27.0	17.7	7.8

Figure 9: Concentration of particle species and precipitation divided by seasons and CTMs. "all_mean" displays the model ensemble. Spring = March, April, May; summer = June, July, August; autumn = September, October, November; winter = December, January, February. Concentration is based on the annual median over the whole domain. Precipitation displays the seasonal sum (in mm).

3.4.2 Wet Deposition

Wet deposition can provide hints about the fate of particles. EMEP does not deliver separate deposition files for individual particle species but for reduced and oxidized nitrogen. Thus, EMEP is not considered when analyzing wet deposition in this study.

Regarding spatial distribution of NH_4^+ wet deposition, highest annual sums are displayed by CMAQ and LOTOS-EUROS (up to 250 mg/m²/year over land; up to 50 mg/m²/year over water; Figure S24). CAMx and CHIMERE show a similar spatial distribution with values mainly between 10 mg/m²/year and 25 mg/m²/year. CAMx and CHIMERE used the same meteorology data, but despite of this the seasonal distribution of wet deposition differs (Figure 10). An explanation of this differing behavior might be provided by the scavenging mechanisms. In CHIMERE the incloud mechanism for deposition of particles is assumed to be proportional to amount of water lost by precipitation. In CAMx, the incloud scavenging coefficient for aqueous aerosols is the same as for the scavenging of cloud droplets. Below the cloud, CHIMERE uses a polydisperse distribution following Henzig et al. (2006) whereas in CAMx for rain or graupel the collection efficiency is calculated as in Seinfeld & Pandis (1998). The other possible explanation is that all the emissions in CAMx are emitted in the first layer and in CHIMERE, it depends on the emissions distribution.

Regarding the wet deposition of sulfate, the annual totals for all emission sources are highest over the Balkan Peninsula in the CMAQ and LOTOS-EUROS model outputs (300 mg/m²/year to 800 mg/m²/year; Figure S25). For CAMx over land areas, the values reach 300 mg/m²/year, and the lowest totals over land can be seen in the CHIMERE results (0.0 mg/m²/year to 50 mg/m²/year). Over water, these values are low in all model outputs (50 mg/m²/year to 150 mg/m²/year), except CHIMERE, contrary to the other models, highest wet deposition was found over water.

The wet deposition of NO_3^- is highest for CMAQ (> 400 mg/m²/year) over the whole domain (Figure S26). For CAMx and LOTOS-EUROS, it is generally lower, with most areas displaying 25 mg/m²/year to 50 mg/m²/year. Lowest wet deposition of nitrate is shown in CHIMERE outputs with values not exceeding 50 mg/m². Regarding the sum for the whole year, the highest values are found for CMAQ (Northern Italy and the Balkan Peninsula, where the urban-area values reached 400 mg/m²/year). Over water, deposition is lower than over land in the results of all CTMs. Lower wintertime precipitation in CMAQ compared to the other models might lead to high particle concentrations as well as high deposition due to low dilution (Figure 10).

Wet deposition depends mainly on the ability of models to predict the amount, duration, and type of precipitation. The precipitation data show that the lowest values are found for CMAQ input data. CAMx and CHIMERE use the same meteorological input data and thus display the same precipitation results, with the highest values in winter. CMAQ and LOTOS-EUROS have precipitation values within a similar range, with the highest values occurring in autumn and winter.

Although the precipitation results in CAMx and CHIMERE are the same, wet deposition differed among these two models, indicating that the concentration as well as model internal mechanisms caused differences rather than the input data. Additionally, in CMAQ, a lower wet deposition rate is expected for nitrate. There are usually two mechanisms important for scavenging in CMAQ; in-cloud and below-cloud scavenging. High wet deposition for nitrate in CMAQ outputs might be traced

back to efficient below cloud scavenging of coarse mode particles containing nitrate, through which the wet deposition can be high despite precipitation in similar ranges as other models. Furthermore, the deposition of particulate nitrate crucially depends on the reactive uptake of HNO_3 to larger particles (Karl et al., 2019), because coarse-mode particles are removed much faster than fine-mode particles.
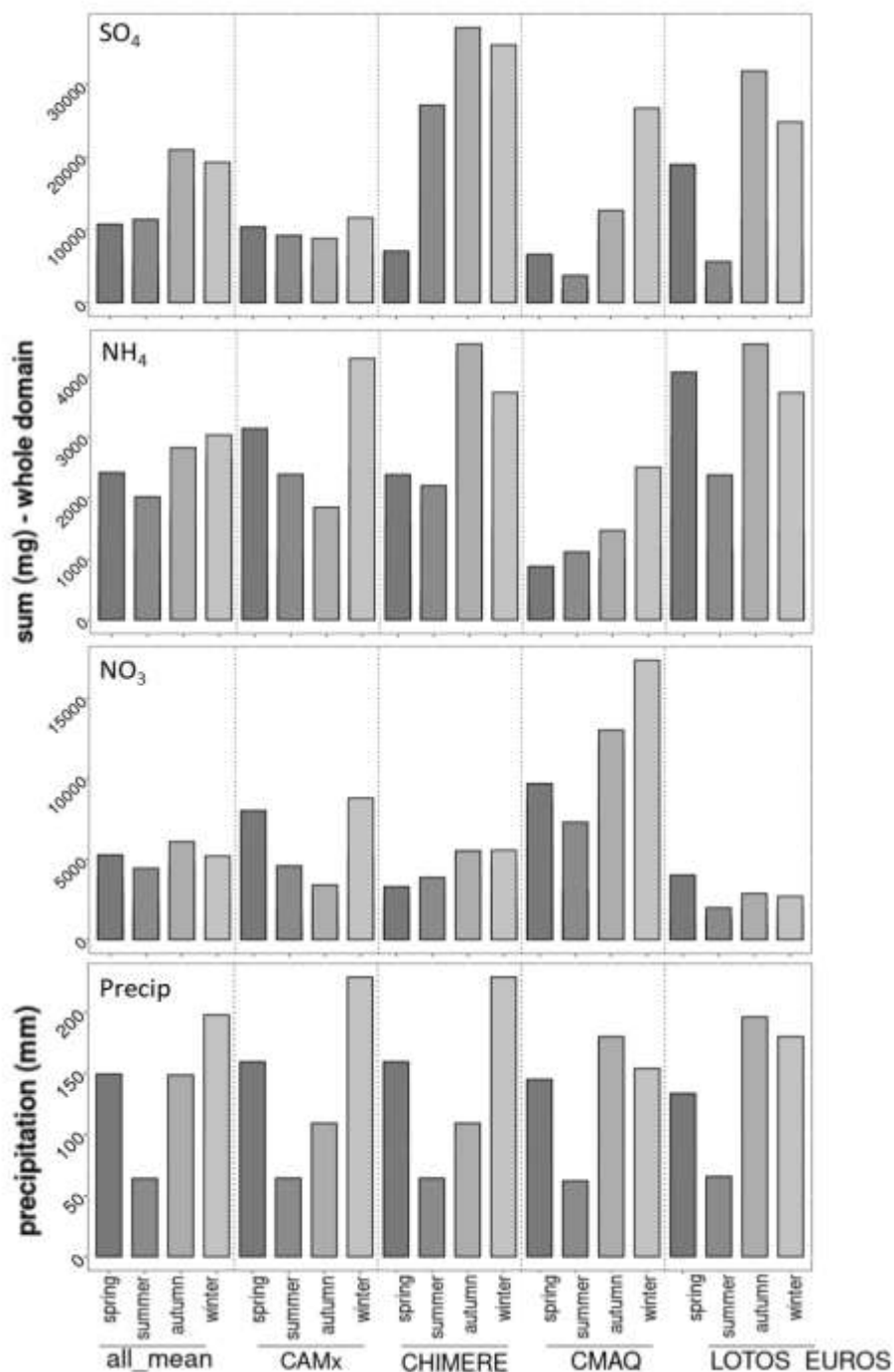
Figure 10: Wet deposition sum (mg/season) of particle species and precipitation divided by seasons and CTMs. "all_mean" displays the model ensemble. Spring = March, April, May; summer = June, July, August; autumn = September, October, November; winter = December, January, February. Wet deposition is based on the annual sum over the whole domain. Precipitation displays the seasonal sum (in mm).

4 Discussion

Various reasons for deviations of PM$_{2.5}$ concentrations among regional CTM systems might be traced back to model-specific calculations.

Regarding PM (coarse and fine for sea salt), an uncertainty among models might be caused by the differences in calculation of sea salt and dust emissions. Here, both is considered in all CTMs, except for dust in CMAQ. If sodium chloride and dust components are not considered, underestimations of PM and uncertainties in areas near coasts (sea salt) or where dust is important, e.g. Saharan dust in the Mediterranean region, occur, as described in Section 3.1. Furthermore, if sea salt and dust are omitted from the pH calculations, it might also cause deviations in sulfur chemistry, as this factor is very sensitive to pH. In the CMAQ runs dust was considered at the model boundaries but dust emissions were not included. The Mediterranean region is frequently affected by Saharan desert dust (Palacios-Peña, 2019), but the main source region for this dust emission is not included in the model domain, thus the dust coming from the boundary can be seen as sufficient for the CMAQ model run. Generally, the boundary conditions for dust and sea salt in CAMx and CHIMERE were produced by offline models that are running on meteorological fields from GEOS-5, GEOS DAS and MERRA. For CMAQ and LOTOS-EUROS these boundary conditions were produced within the boundary conditions calculations. Boundary conditions of EMEP are developed from climatological ozone-sonde datasets.

All models used offline meteorology in which the ABL heights were calculated. Annual medians of the atmospheric boundary layer heights at 4 PM and 4 AM were compared among the models. The comparison of spatial distribution of ABL heights at 4 PM and 4 AM shows that over water, the ABL heights have not much variability in all models (Figure S27 and S28). The lowest ABL height over water was used for CHIMERE. This corresponds to the high PM$_{2.5}$ concentrations simulated by this model over water. Over land, the comparison of spatial distribution at 4 PM to 4 AM display more variable ABL heights: during nighttime the ABL heights are up to 200 m whereas during daytime the heights increase to 1000 m or higher (Figure S27 and S28). Over land the input in CAMx, CHIMERE, CMAQ and LOTOS-EUROS has a higher median ABL at 4 PM whereas in EMEP it is contrary with showing highest median at 4 PM mainly over water areas. Yet, there was no large deviation in PM$_{2.5}$ concentration simulated by EMEP to concentrations received from other models. Generally, due to ABL dynamics deviations from measured to simulated data can be expected because measurement stations were chosen close to the coast, which leads to uncertainties. In these areas, the measurements are influenced by air masses either coming from water or coming from land. In addition, measured data was received from one measurement point, which is hardly representative for a whole grid cell of 12 x 12 km².

The treatment of dust, sea salt and the used boundary conditions have an effect on the analysis and comparison of PM results, because these parameters part of the PM$_{2.5}$ formation but differ among the models. Regarding the CTMs performance, reasons for underestimations of PM$_{2.5}$ were already discussed in previous studies: For CAMx, Pepe et al. (2019) linked these underestimations to meteorological parameters and to the overestimation of the vertical mixing in the lower atmosphere. Tuccella et al. (2019) found underestimations of PM$_{2.5}$ in the CHIMERE model and explained

these by an excess of wet scavenging in the model. An excess of wet scavenging in CHIMERE compared to the other CTM systems is not found in the present study, thus it cannot be used as explanation for deviations here. In EMEP, differing from the other CTM systems, the MARS module was used to calculate the equilibrium between the gas and aerosol phases; this model does not treat sea salt or dust, leading to underestimations of $PM_{2.5}$. Kranenburg et al. (2013) linked the underestimation of particulate matter in LOTOS-EUROS to the missing descriptions of SOA processes in the model. Thus, various reasons and combinations of reasons can lead to underestimations of $PM_{2.5}$ in the CTM systems used herein. For a better understanding, the inorganic particle species are considered in the present study. Consideration of inorganic as well as organic particles could lead to more uncertainties. Besides, in shipping emissions the inorganic aerosols display a higher share.

Large part of $PM_{2.5}$ is secondary, therefore underestimations can be linked to underestimations of precursors, e.g., NO_2. This was already shown in the first part of this intercomparison study, where all five CTM systems underestimated measured NO_2 (Fink et al., 2023). But also SO_2 is usually underestimated by CTMs, as shown in previous studies (e.g. Eyring et al., 2007).

Four out of five CTM systems underestimate the actual measured $PM_{2.5}$ concentration in the present study. Gaseous precursors like SO_2 and NO_2 need to be oxidized before they can form particles in reactions with ammonia. The hydroxyl radical (OH) is the main oxidant. The amount of available OH can be analyzed when the NO_2 concentration is set in relation to HNO_3 and NO_3^- (Figure S24).This gives an indication about the OH availability. In ship plumes OH is consumed fast, therefore values are low along the shipping lanes. In regions with lower NO_2 concentration more OH is available and HNO_3 is efficiently formed. In the present study, the HNO_3 was similar within all five CTM systems (Figure S5).

One reason for the differences in HNO_3 might be traced back to the amount of cloud droplets, since HNO_3 is resolved in it. The dissolution of gases in droplets is usually assumed to be irreversible for HNO_3 and NH_3 in CTMs; thus, the amount of formed ammonium nitrate mass depends on the amount of HNO_3 or the cloud droplets. This could lead in the end to the deviation among the CTMs simulated HNO_3.

The preference of NH_4^+ to bind to SO_4^{2-} in atmospheric aerosols to form $(NH_4)_2SO_4$ explains why in some models NO_3^- displays relatively low values when the SO_4^{2-} concentration is high. CHIMERE, for instance, has a NO_3^- share of 3.1 % to total $PM_{2.5}$ and a SO_4^{2-} share of 27.0 %, whereas in the CAMx results, NO_3^- had a share of 11.1 % to total $PM_{2.5}$ and a SO_4^{2-} share of 14.6 %. This can be confirmed by the low SO_2 concentration and high SO_4^{2-} concentration in CHIMERE (Figures S12 & S20), indicating that sulfate is formed more efficiently compared to CAMx. Furthermore, this leads to lower NO_3^- concentration in CHIMERE output (Figure S22). Also for SO_2 and SO_4^{2-} concentration cloud water and amount of cloud droplets plays an important role.

Regarding the thermodynamic equilibrium within the models, ISORROPIA and ISORROPIA II mechanisms are used in all CTM systems except EMEP, meaning similar results can be assumed to be obtained from this mechanism. Despite this similarity, differences in concentrations may be a result of differences in available cloud water, vertical mixing, the spatiotemporal distribution of emissions or aerosol size distributions. EMEP uses the MARS module to calculate the equilibrium between the gas and the aerosol phase. Although four of five models use the ISORROPIA or ISORROPIA II

mechanisms for inorganic secondary aerosol formation, many factors within these models still cause significant differences among the model outputs.

The aerosol size distribution also has an impact on the particle species distribution. As displayed in Table 1 (Section 2.1), there are two concepts how the aerosol size distribution is represented within the models, either the distribution in bins or in log-normal modes. As already discussed in Solazzo et al. (2012) the PM chemical composition differs greatly with the particle size. Consequently, differences in modelling the aerosol size distribution also affects the chemical composition. In CMAQ, for example, large fractions of nitrate and ammonium can be found in the coarse mode where they undergo other removal processes than in the fine mode.

Although there is harmonization in terms of the input emission data in the present study, the internal model mechanisms used to calculate particulate matter lead to differences in the particle species distribution, as discussed in Sect. 3.1. In addition, the calculations how to determine $PM_{2.5}$ vary among CTM systems or even within one CTM. As an example, there are two possibilities for calculating $PM_{2.5}$ within CMAQ: either online during the model run with the $PM_{2.5}$ module or subsequently by calculating the value as the sum of two modes. These different options lead to different results (as shown by Jiang et al., 2006) and will also affect the particle composition. In the present study, the sum of two modes is used in CMAQ. Model simulations with relatively high $PM_{2.5}$ concentrations display higher absolute shipping impacts on $PM_{2.5}$, as presented in Sect. 3.2. Consequently, relatively low variability in the relative potential ship impacts among the models compared to that of the absolute values could be expected. For a more quantitative evaluation, relative potential ship impact is plotted against absolute potential impact. A larger incline of the regression line can be explained by a higher background $PM_{2.5}$ concentration, thus relative ship impact is lower for the same concentration increase (e.g. EMEP and CHIMERE) (Figure S30).

From the ISORROPIA and ISORROPIA II mechanism, it can be expected that the molar ratios between the acids on the one side (NO_3^- and SO_4^{2-}) and the base on the other side (NH_4^+) are in balance. However, the ratio between SO_4^{2-}, NH_4^+ and NO_3^- shows that the balance in all models expect LOTOS-EUROS is not given for $PM_{2.5}$; sulfate plus nitrate is much higher compared to ammonium (Figure S31). This balance is almost perfectly given in LOTOS-EUROS, although both, CMAQ and LOTOS-EUROS, used the ISORROPIA II mechanism. Especially at the shipping lanes, an imbalance among the inorganic particle species is present. Differences of particle species ratio among the models can be traced back to the differences in particle size distribution. Contrary to the other models, CAMx has only three species in the coarse mode: coarse others primary, coarse crustal and reactive gaseous mercury. For NO_3^- and SO_4^{2-}, the ratio between the fine and coarse mode is calculated for the CTMs (Figure S32 & S33). NH_4^+ was not considered here, since it is only in present in coarse mode in CMAQ. These ratios show that CHIMERE and LOTOS-EUROS have only a small proportion of particles in coarse mode. For SO_4^{2-} in LOTOS-EUROS the coarse particle concentration is zero and for EMEP no SO_4^{2-} is present in coarse mode. In CMAQ a higher concentration of particles is assigned to the coarse mode, also for NH_4^+.

The present study has shown that different reasons can cause deviations among the simulated $PM_{2.5}$ CTM outputs. Major reasons are the differences in size distribution and how models distribute chemical species among the coarse and fine mode ($PM_{2.5}$ and PM_{10}). Differences among the modelled $PM_{2.5}$ concentrations can also be a result of the differences in the height of

the lowest model layer and the way in which ship emissions are distributed among the layers. As shown in Fink et al. (2023) the vertical distribution of $PM_{2.5}$ precursor emissions varies among the models, e.g. in CAMx all shipping emissions are assigned to the lowest layer. This leads to differences in chemical transformations because of different concentration levels close to the source and consequently to deviations among the particle distributions. Furthermore, precipitation differences lead

635   to variations among the model outputs for wet deposition.

Limitations of the present study are that only the chemistry of the lowest layer is evaluated. The model input was standardized as far as possible, but meteorological input data varied and is not compared in detail here. Interactions between fine and coarse particles are only studied to a limited extent, the same holds for aqueous chemistry, which has an impact on oxidation mechanisms of sulphur species.

640

5 Summary and Conclusion

The current work investigates and analyzes the predictions of five different CTM systems for $PM_{2.5}$ and inorganic particle species (NH_4^+, SO_4^{2-}, NO_3^-) dispersion and transformation in the Mediterranean region. Beside the total concentration focus is laid on the potential ship impact. Results show that four of the five models underestimated the actual measured $PM_{2.5}$ concentrations at stations close to the European coastline. The relative ship impacts on $PM_{2.5}$ simulated by the CTMs at the measurement stations are between 5.7 % (CMAQ) and 13.8 % (CAMx). The potential impact of $PM_{2.5}$ from ships simulated by CAMx, LOTOS-EUROS and EMEP have the largest areas with values up to 25 % along main shipping routes in the Mediterranean Sea. CMAQ and CHIMERE simulated potential ship impacts of 15 % along the main shipping lines close to the African coast. These impacts are within the range of the ship impacts obtained in other studies.

The spatial distribution of ammonium displays a low total annual mean mainly in the southwestern part of the domain (approximately 0.0 µg/m³) and is highest in the Po Valley and Bosporus (1.5 µg/m³). The ensemble mean of NH_4^+ (0.6 µg/m³) is in good agreement with the measurements provided in previous studies. The relative and absolute ship impacts are very similar for all models (0.0 µg/m³ to 0.06 µg/m³ over land, up to 0.15 µg/m³ over water; 0.25 % to 5.0 % over land, and 10 % to 25 % over water). This indicates that differences among the simulated $PM_{2.5}$ from ships result from differences in sulfate and nitrate.

The NH_4^+ proportion to total $PM_{2.5}$ is similar in all models (5.6 % to 7.8 %), and only LOTOS-EUROS shows a relatively high share (12.2 %). The ship impact pattern is similar; all models display proportions between 9.1 % and 12.6 %, but higher values are simulated by LOTOS-EUROS (23.5 %).

SO_4^{2-} is main contributor to the total $PM_{2.5}$ concentration regarding shipping emissions only. In the model ensemble mean for the absolute ship concentration, SO_4 2- accounts for 44.6 % of $PM_{2.5}$. The annual mean sulfate total concentration is highest for CHIMERE in the eastern part of the domain, reaching 6.0 µg/m³. CAMx, CMAQ, EMEP and LOTOS-EUROS simulate a total SO_4^{2-} concentration within one range between 0.4 µg/m³ and 2.0 µg/m³ in the western part of the domain. The relative potential ship impacts on total SO_4^{2-} are lowest over land, with values up to 3.0 %, and higher in coastal areas, with values ranging from 6 % to 20 %. Along the main shipping routes, the impacts are highest, reaching 50 % for CAMx, EMEP and LOTOS-EUROS; for CHIMERE and CMAQ, they are lower, with values reaching 30 %. Regarding the absolute ship impacts on SO_4^{2-}, the model simulations display similar concentrations and are slightly lower for CMAQ and LOTOS-EUROS. Especially over water areas with relatively high SO_2 and SO_4^{2-} concentrations are identified. Because NH_4^+ preferentially binds to SO_4 2- in atmospheric aerosols to form $(NH_4)_2SO_4$, in areas over water less NH_4NO_3 forms.

The highest annual mean NO_3^- total concentrations appear over land areas in the simulations by CAMx, CMAQ and LOTOS-EUROS, especially over Italy and in the Balkan states (> 2 µg/m³). The lowest concentrations are simulated by CHIMERE. The concentrations over water are lower than those over land areas. The ensemble mean of all CTMs over the whole domain shows a median value of 0.63 µg/m³. Higher concentrations over land than over water are expected due to NH_4NO_3 formation in areas characterized by high NH_3 and HNO_3 conditions and low SO_4^{2-} conditions.

The relative potential ship impact on NO_3^- differs among the models. The CAMx, EMEP and LOTOS-EUROS results are similar; the relative potential ship impacts over land ranges from 0.0 % to 5.0 % (in the Balkan states), those in coastal areas and Italy ranges from 10 % to 25 % and those along main shipping routes from 50 % to 65 % or reaches even 85 %. CHIMERE and CMAQ show lower relative potential ship impacts for NO_3^-. For CMAQ, the impacts are lowest along the main shipping routes, nitrate is even reduced by 25 %. Low values in nitrate can be explained by the preference to form $(NH_4)_2SO_4$, thus nitrate stays in the gas phase or is transferred to the coarse mode. These low values for SO_4^{2-} und NO_3^- in CMAQ but relatively high values for EMEP, CAMx and LOTOS are reflected in the $PM_{2.5}$ ship impacts and partly explain the deviations in $PM_{2.5}$ among the models. As expected the seasonal variabilities in particle species show that SO_4^{2-} and NH_4^+ are less temperature-dependent than NO_3^-. Nitrate is higher in winter and spring, but lower in summer and autumn. This pattern is found in all CTM simulations.

The spatial distribution of NH_4^+ wet deposition shows highest annual sums by CMAQ and LOTOS-EUROS (up to 250 mg/m²/year over land; up to 50 mg/m²/year over water). CAMx and CHIMERE show a similar spatial distribution with values mainly between 10 mg/m²/year and 25 mg/m²/year. For wet deposition of SO_4^{2-}, the annual totals for all emission sources are highest over the Balkan Peninsula in the CMAQ and LOTOS-EUROS model outputs (300 mg/m²/year to 800 mg/m²/year). For CAMx over land areas, the values reach 300 mg/m²/year, and the lowest totals over land can be seen in the CHIMERE results (0.0 mg/m²/year to 50 mg/m²/year). Over water, these values are low in all model outputs (50 mg/m²/year to 150 mg/m²/year), except CHIMERE. The wet deposition of NO_3^- is highest for CMAQ (> 400 mg/m²/year) over the whole domain. For CAMx and LOTOS-EUROS, it is generally lower, with most areas displaying 25 mg/m²/year to 50 mg/m²/year. Lowest wet deposition of nitrate is shown in CHIMERE outputs with values not exceeding 50 mg/m². Over water, deposition is lower than over land in the results of all CTMs.

The complexity of particle treatments within the models, as well as the large number of causes of these changes make it difficult to find a single cause for the variable outputs. One point causing uncertainties is that the aerosol-formation mechanisms differ among CTMs. The detailed investigation of $PM_{2.5}$ and its chemical composition has demonstrated that differences among the particle species might be traced back to the aerosol size distribution. This was shown especially for CMAQ regarding the balance of the inorganic particle species nitrate and sulphate on the one side and ammonium on the other side. CMAQ and EMEP tend to assign a higher particle mass to the coarse mode compared to the other three CTMs. This has implications for particle deposition because both, wet and dry deposition are more efficient for larger particles.

An ensemble mean with standard deviations based on several model results can provide a more reliable assessment of possible ship impacts on air concentration and deposition. Previous research has demonstrated that using only one chemical transport model resulted in underestimated model uncertainty and overconfidence in the conclusions (e.g., Solazzo et al., 2013; Riccio et al., 2012; Solazzo et al., 2018), indicating that a model ensemble should better be used. Particularly in terms of the study's policy point of view, the ensemble mean is important: If model simulations are used to support in decision-making regarding shipping regulations, the uncertainty of individual models must be considered.

Goal of this study was not to make model outputs as similar as possible, but to show the discrepancies that occur among CTM systems despite using similar input data. Different CTM systems were asked the same question to find the impact of shipping for which they got the same emissions as input data.

710 Nevertheless, to achieve less varying results in future studies, the vertical emission distribution as well as the boundary conditions could be the same in all CTM inputs. This can help to make the modeled output more alike. Adjustments in using the same meteorology could be also helpful yet difficult to realize, since the meteorology and meteorological driver within each CTM system is closely connected. To better insight in certain mechanisms, one model could be used with e.g. changing vertical profiles, emissions or meteorology. Furthermore, the present study neither use the same boundary conditions, nor did

715 the models use the same sea salt or dust emissions. For more consistent investigations of model results this future intercomparison studies should be carried out with using the same boundary conditions, sea salt and dust emissions as input data.

Regional-scale models with relatively coarse grid resolutions do not account for chemical transformation mechanisms within a ship's exhaust gas plume. They typically assume direct dilution and neglect the in-plume chemistry at high pollutant

720 concentration levels. To obtain more precise information regarding effects of shipping on particle concentrations, the particle size distribution and the interaction mechanisms from plume to background concentrations, as well as chemical transformations within ship plumes should be considered in future studies.

Code and data availability

CAMx source code and documentation can be downloaded from https://camx-wp.azurewebsites.net/download/source/ (last access: 19 January 2023; Ramboll, 2023) and the Chimere website (https://www.lmd.polytechnique.fr/chimere/2020_getcode.php, last access: 19 January 2023). CMAQ version 5.2, which was used here, is available at https://doi.org/10.5281/zenodo.1167892 (US EPA Office of Research and Development, 2017). EMEP is available at https://doi.org/10.5281/zenodo.3647990 (EMEP MSC-W, 2020), LOTOS-EUROS is available at https://lotos-euros.tno.nl/open-source-version/ (last access: 19 January 2023; TNO, 2023), and WPS/WRF is available from WPS (2022; https://github.com/wrf-model/WPS, last access: 19 January 2023) and WRF Community (2000, https://doi.org/10.5065/D6MK6B4K). The COSMO software is available at https://www.cosmo-model.org/content/support/software/default.htm#models (last access: 24 January 2023; COSMO, 2023) and ecmwf-ifs/ifs-scripts at https://github.com/ecmwf-ifs (last access: 19 January 2023; ECMWF, 2023).

Data on measurement stations from EEA can be downloaded at https://discomap.eea.europa.eu/map/fme/AirQualityExport.htm (last access: 20 January 2023). CTM model results are available upon request.

Author contributions

LF: CMAQ model runs, evaluation and analysis of model results, preparation and writing of the paper. MK: Analysis of the results, revision of the text. VM: Supervision, analysis of the results, revision of the text. SO: CAMx and CHIMERE model runs, discussion of the results. RK and JK: LOTOS-EUROS model runs, land-based emissions data provision, discussion of the results. JM and SJ: EMEP model runs, discussion of the results. JPJ and EM: STEAM model runs, shipping emissions data provision, discussion of the results.

Competing interests

The contact author has declared that none of the authors has any competing interests.

Acknowledgements

760 **References**

Agrawal, H., Eden, R., Zhang, X., Fine, P. M., Katzenstein, A., Miller, J. W., Ospital, J., Teffera, S., and Cocker, D. R.: Primary particulate matter from ocean-going engines in the Southern California Air Basin, Environ. Sci. Technol. 2009, 43, 14, 5398–5402, https://doi.org/10.1021/es8035016, 2009.

Agrawal, H., Welch, W. A., Henningsen, S., Miller, J. W., and Cocker, D. R.: Emissions from main propulsion engine on
765 container ship at sea, J. Geophys. Res, 115, D23205, https://doi.org/10.1029/2009JD013346, 2010.

Agrawal, H., Welch, W. A., Miller, J. W., and Cockert, D. R.: Emission measurements from a crude oil tanker at sea, Environ. Sci. Technol. 2008, 42(19), 7098–7103, https://doi.org/10.1021/es703102y, 2008.

Aksoyoglu, S., Baltensperger, U., and Prévôt, A. S. H.: Contribution of ship emissions to the concentration and deposition of air pollutants in Europe, Atmos. Chem. Phys., 16, 1895–1906, https://doi.org/10.5194/acp-16-1895-2016, 2016.

770 Alfaro, S. D. and Gomes, L.: Modeling mineral aerosol production by wind erosion: Emission intensities and aerosol size distributions in source areas., J. Geophys. Res., 106, 18075–18084, doi:10.1029/2000jd900339, 2001.

Appel, K. W., Foley, K. M., Bash, J. O., Pinder, R. W., Dennis, R. L., Allen, D. J., and Pickering, K.: A multi-resolution assessment of the Community Multiscale Air Quality (CMAQ) model v4.7 wet deposition estimates for 2002–2006, Geosci. Model Dev., 4, 357–371, https://doi.org/10.5194/gmd-4-357-2011, 2011.

775 Appel, K. W., Napelenok, S. L., Foley, K. M., Pye, H. O. T., Hogrefe, C., Luecken, D. J., Bash, J. O., Roselle, S. J., Pleim, J. E., Foroutan, H., Hutzell, W. T., Pouliot, G. A., Sarwar, G., Fahey, K. M., Gantt, B., Gilliam, R. C., Heath, N. K., Kang, D., Mathur, R., Schwede, D. B., Spero, T. L., Wong, D. C., and Young, J. O.: Description and evaluation of the Community Multiscale Air Quality (CMAQ) modeling system version 5.1, Geosci. Model Dev., 10, 1703–1732, https://doi.org/10.5194/gmd-10-1703-2017, 2017.

780 Astitha, M., Lelieveld, J., Abdel Kader, M., Pozzer, A., and Meij, A. de: Parameterization of dust emissions in the global atmospheric chemistry-climate model EMAC: impact of nudging and soil properties, Atmos. Chem. Phys., 12, 11057–11083, https://doi.org/10.5194/acp-12-11057-2012, 2012.

Baldasano, J. M., Pay, M. T., Jorba, O., Gassó, S., and Jiménez-Guerrero, P.: An annual assessment of air quality with the CALIOPE modeling system over Spain, Sci. Total Environ., 409(11), 2163-2178,
785 https://doi.org/10.1016/j.scitotenv.2011.01.041, 2011.

Balzarini, A., Pirovano, G., Honzak, L., Žabkar, R., Curci, G., Forkel, R., Hirtl, M., San José, R., Tuccella, P., and Grell, G. A.: WRF-Chem model sensitivity to chemical mechanisms choice in reconstructing aerosol optical properties, Atmos. Environ.,, 115, 604-619, https://doi.org/10.1016/j.atmosenv.2014.12.033, 2015.

790   Banzhaf, S., Schaap, M., Kerschbaumer, A., Reimer, E., Stern, R., van der Swaluw, E., and Builtjes, P.: Implementation and evaluation of pH-dependent cloud chemistry and wet deposition in the chemical transport model REM-Calgrid, Atmos. Environ., 49, 378-390, https://doi.org/10.1016/j.atmosenv.2011.10.069, 2012.

Barbu, A. L., Segers, A. J., Schaap, M., Heemink, A. W., and Builtjes, P.J.H.: A multi-component data assimilation experiment directed to sulphur dioxide and sulphate over Europe, Atmos. Environ., 43(9), 1622-1631, https://doi.org/10.1016/j.atmosenv.2008.12.005, 2009.

795   Behera, S.N., Sharma, M., Aneja, V.P. et al. Ammonia in the atmosphere: a review on emission sources, atmospheric chemistry and deposition on terrestrial bodies. Environ Sci. Pollut. Res. 20, 8092–8131, https://doi.org/10.1007/s11356-013-2051-9, 2013

Benish, S. E., Bash, J. O., Foley, K. M., Appel, K. W., Hogrefe, C., Gilliam, R., and Pouliot, G.: Long-term regional trends of nitrogen and sulfur deposition in the United States from 2002 to 2017, Atmos. Chem. Phys., 22, 12749–12767, 800   https://doi.org/10.5194/acp-22-12749-2022, 2022.

Berge, E. and Jakobsen, H. A.: A regional scale multilayer model for the calculation of long-term transport and deposition of air pollution in Europe, Tellus B, 50(3), https://doi.org/10.1034/j.1600-0889.1998.t01-2-00001.x, 1998.

Bergström, R., Denier van der Gon, H. A. C., Prévôt, A. S. H., Yttri, K. E., and Simpson, D.: Modelling of organic aerosols over Europe (2002–2007) using a volatility basis set (VBS) framework: application of different assumptions regarding the 805   formation of secondary organic aerosol, Atmos. Chem. Phys., 12, 8499–8527, https://doi.org/10.5194/acp-12-8499-2012, 2012.

Bieser, J., Aulinger, A., Matthias, V., Quante, M., and van der Denier Gon, H. A. C.: Vertical emission profiles for Europe based on plume rise calculations, Environ. Pollut., 159(10), 2935-2946, https://doi.org/10.1016/j.envpol.2011.04.030, 2011.

Binkowski, F. S. and Shankar, U.: The Regional Particulate Matter Model: 1. Model description and preliminary results, J. 810   Geophys. Res., 100(D12), 26,191-26,209, https://doi.org/10.1029/95JD02093, 1995.

Binkowski, F. S. and Roselle, S. J.: Models-3 Community Multiscale Air Quality (CMAQ) model aerosol component 1. Model description, J. Geophys. Res., 108(D6), https://doi.org/10.1029/2001JD001409, 2003.

Byun, D. and Schere, K. L.: Review of the Governing Equations, Computational Algorithms, and Other Components of the Models-3 Community Multiscale Air Quality (CMAQ) Modeling System, Appl. Mech. Rev., 2, 815   https://doi.org/10.1115/1.2128636, 2006.

Carlton, A. G., Bhave, P. V., Napelenok, S. L., Edney, E. O., Sarwar, G., Pinder, R. W., Pouliot, G. A., and Houyoux, M.: Model representation of secondary organic aerosol in CMAQv4.7, Appl. Mech. Rev., 59(2), 51–77, https://doi.org/10.1021/es100636q, 2010.

Celik, S., Drewnick, F., Fachinger, F., Brooks, J., Darbyshire, E., Coe, H., Paris, J.-D., Eger, P. G., Schuladen, J., Tadic, I., 820   Friedrich, N., Dienhart, D., Hottmann, B., Fischer, H., Crowley, J. N., Harder, H., and Borrmann, S.: Influence of vessel characteristics and atmospheric processes on the gas and particle phase of ship emission plumes: In situ measurements in the Mediterranean Sea and around the Arabian Peninsula, Atmos. Chem. Phys., 20, 4713–4734, https://doi.org/10.5194/acp-20-4713-2020, 2020

Chen, R., Hu, B., Liu, Y., Xu, J., Yang, G., Xu, D., and Chen, C.: Beyond PM2.5: The role of ultrafine particles on adverse health effects of air pollution, Biochim Biophys Acta, 1860(12), 2844-2855, https://doi.org/10.1016/j.bbagen.2016.03.019, 2016.

Clappier, A., Thunis, P., Beekmann, M., Putaud, J. P., and Meij, A. de: Impact of SOx, NOx and NH3 emission reductions on PM2.5 concentrations across Europe: Hints for future measure development, Environ. Int.,156, 106699, https://doi.org/10.1016/j.envint.2021.106699, 2021.

Corbett, J. J. and Fischbeck, P.: Emissions from ships, Science 278 (5339), 823- 824, 1997.

Donahue, N. M., Robinson, A. L., and Pandis, S. N.: Atmospheric organic particulate matter: From smoke to secondary organic aerosol, Atmos. Environ, 43(1), 94-106, https://doi.org/10.1016/j.atmosenv.2008.09.055, 2009.

Donateo, A., Gregoris, E., Gambaro, A., Merico, E., Giua, R., Nocioni, A., and Contini, D.: Contribution of harbour activities and ship traffic to PM2.5, particle number concentrations and PAHs in a port city of the Mediterranean Sea (Italy), Environ. Sci. Pollut. Res., 21, 9415–9429, https://doi.org/10.1007/s11356-014-2849-0, 2014.

Emberson, L. D., Simpson, D., Tuovinen, J.-P., Ashmore, M. R. and Cambridge, H. M.: 'Towards a Model of Ozone Deposition and Stomatal Uptake over Europe', EMEP/MSC-W Note 6/00, Norwegian Meteorological Institute, Oslo, 57, 2000.

EMEP Status Report 1/2022. "Transboundary particulate matter, photo-oxidants, acidifying and eutrophying components". Joint MSC-W & CCC & CEIP & CIAM Report. https://emep.int/publ/reports/2022/EMEP_Status_Report_1_2022.pdf, 2022.

Erisman, J. W., van Pul, A., and Wyers, P.: Parametrization of surface resistance for the quantification of atmospheric deposition of acidifying pollutants and ozone, Atmos. Environ., 28(16), 2595-2607, https://doi.org/10.1016/1352-2310(94)90433-2, 1994.

Eyring, V.: Emissions from international shipping: 1. The last 50 years, J. Geophys. Res., 110(D17), https://doi.org/10.1029/2004JD005619, 2005.

Eyring, V., Stevenson, D. S., Lauer, A., Dentener, F. J., Butler, T., Collins, W. J., Ellingsen, K., Gauss, M., Hauglustaine, D. A., Isaksen, I. S. A., Lawrence, M. G., Richter, A., Rodriguez, J. M., Sanderson, M., Strahan, S. E., Sudo, K., Szopa, S., van Noije, T. P. C., and Wild, O.: Multi-model simulations of the impact of international shipping on Atmospheric Chemistry and Climate in 2000 and 2030, Atmos. Chem. Phys., 7, 757–780, https://doi.org/10.5194/acp-7-757-2007, 2007.

Fécan, F., Marticorena, B., and Bergametti, G.: Parameterization of the increase of aeolian erosion threshold wind friction velocity due to soil moisture for arid and semi-arid areas, Ann. Geophys. 17, 149–157, DOI:10.1007/s00585-999-0149-7, 1999.

Fink, L., Karl, M., Matthias, V., Oppo, S., Kranenburg, R., Kuenen, J., Moldanova, J., Jutterström, S., Jalkanen, J.-P., and Majamäki, E.: Potential impact of shipping on air pollution in the Mediterranean region – a multimodel evaluation: comparison of photooxidants NO2 and O3, Atmos. Chem. Phys., 23, 1825–1862, https://doi.org/10.5194/acp-23-1825-2023, 2023.

Folberth, G. A., Hauglustaine, D. A., Lathière, J., and Brocheton, F.: Interactive chemistry in the Laboratoire de Météorologie Dynamique general circulation model: model description and impact analysis of biogenic hydrocarbons on tropospheric chemistry, Atmos. Chem. Phys., 6, 2273–2319, https://doi.org/10.5194/acp-6-2273-2006, 2006.

Foley, K. M., Roselle, S. J., Appel, K. W., Bhave, P. V., Pleim, J. E., Otte, T. L., Mathur, R., Sarwar, G., Young, J. O., Gilliam, R. C., Nolte, C. G., Kelly, J. T., Gilliland, A. B., and Bash, J. O.: Incremental testing of the Community Multiscale Air Quality (CMAQ) modeling system version 4.7, Geosci. Model Dev., 3, 205–226, https://doi.org/10.5194/gmd-3-205-2010, 2010.

Fountoukis, C. and Nenes, A.: ISORROPIA II: A computationally efficient thermodynamic equilibrium model for K+–Ca2+–Mg2+–NH4+–Na+–SO42−–NO3−–Cl−–H2O aerosols, Atmos. Chem. Phys., 7, 4639–4659, https://doi.org/10.5194/acp-7-4639-2007, 2007.

865 Friedrich, N., Eger, P., Shenolikar, J., Sobanski, N., Schuladen, J., Dienhart, D., Hottmann, B., Tadic, I., Fischer, H., Martinez, M., Rohloff, R., Tauer, S., Harder, H., Pfannerstill, E. Y., Wang, N., Williams, J., Brooks, J., Drewnick, F., Su, H., Li, G., Cheng, Y., Lelieveld, J., and Crowley, J. N.: Reactive nitrogen around the Arabian Peninsula and in the Mediterranean Sea during the 2017 AQABA ship campaign, Atmos. Chem. Phys., 21, 7473–7498, https://doi.org/10.5194/acp-21-7473-2021, 2021.

Gao, R. and Sang, N.: Quasi-ultrafine particles promote cell metastasis via HMGB1-mediated cancer cell adhesion, Environ. 870 Pollut., 256, 113390, https://doi.org/10.1016/j.envpol.2019.113390, 2020.

Gašparac, G., Jeričević, A., Kumar, P., and Grisogono, B.: Regional-scale modelling for the assessment of atmospheric particulate matter concentrations at rural background locations in Europe, Atmos. Chem. Phys., 20, 6395–6415, https://doi.org/10.5194/acp-20-6395-2020, 2020.

Ge, Y., Heal, M. R., Stevenson, D. S., Wind, P., and Vieno, M.: Evaluation of global EMEP MSC-W (rv4.34) WRF (v3.9.1.1) 875 model surface concentrations and wet deposition of reactive N and S with measurements, Geosci. Model Dev., 14, 7021–7046, https://doi.org/10.5194/gmd-14-7021-2021, 2021.

Ginoux, P., Chin, M., Tegen, I., Prospero, J. M., Holben, B., Dubovik, O., and Lin, S.-J. (2001), Sources and distributions of dust aerosols simulated with the GOCART model, J. Geophys. Res., 106(D17), 20255– 20273, doi:10.1029/2000JD000053.

Gomes, L., Rajot, J. L., Alfaro, S. C., and Gaudichet, A.: Validation of a dust production model from measurements performed 880 in semi-arid agricultural areas of Spain and Niger, Catena, 52, 257–271, 2003.

Granier, C., Darras, S., van der Denier Gon, H., Doubalova, J., Elguindi, N., Galle, B., Gauss, M., Guevara, M., Jalkanen, J.-P., Kuenen, J., Liousse, C., Quack, B., Simpson, D., and Sindelarova, K.: The Copernicus Atmosphere Monitoring Service global and regional emissions: (April 2019 version), Copernicus Atmosphere Monitoring Service (CAMS) report, https://doi.org/10.24380/d0bn-kx16, 2019.

885 Hauglustaine, D. A., Balkanski, Y., and Schulz, M.: A global model simulation of present and future nitrate aerosols and their direct radiative forcing of climate, Atmos. Chem. Phys., 14, 11031–11063, https://doi.org/10.5194/acp-14-11031-2014, 2014.

Heusinkveld, H. J., Wahle, T., Campbell, A., Westerink, R. H. S., Tran, L., Johnston, H., Stone, V., Cassee, F. R., and Schins, R. P. F.: Neurodegenerative and neurological disorders by small inhaled particles, NeuroToxicology, 56, 94-106, https://doi.org/10.1016/j.neuro.2016.07.007, 2016.

890 Im, U., Christodoulaki, S., Violaki, K., Zarmpas, P., Kocak, M., Daskalakis, N., Mihalopoulos, N., and Kanakidou, M.: Atmospheric deposition of nitrogen and sulfur over southern Europe with focus on the Mediterranean and the Black Sea, Atmos. Environ., 81, 660-670, https://doi.org/10.1016/j.atmosenv.2013.09.048, 2013.

Im, U., Bianconi, R., Solazzo, E., Kioutsioukis, I., Badia, A., Balzarini, A., Baró, R., Bellasio, R., Brunner, D., Chemel, C., Curci, G., van der Denier Gon, H., Flemming, J., Forkel, R., Giordano, L., Jiménez-Guerrero, P., Hirtl, M., Hodzic, A., Honzak, 895 L., Jorba, O., Knote, C., Makar, P. A., Manders-Groot, A., Neal, L., Pérez, J. L., Pirovano, G., Pouliot, G., San Jose, R., Savage, N., Schroder, W., Sokhi, R. S., Syrakov, D., Torian, A., Tuccella, P., Wang, K., Werhahn, J., Wolke, R., Zabkar, R., Zhang, Y., Zhang, J., Hogrefe, C., and Galmarini, S.: Evaluation of operational online-coupled regional air quality models over Europe and North America in the context of AQMEII phase 2. Part II: Particulate matter, Atmos. Environ., 115, 421-441, https://doi.org/10.1016/j.atmosenv.2014.08.072, 2015.

IMO (International Maritime Organization): Guidelines for consistent implementation of the 0.50 % Sulphur limit under Marpol annex VI. Resolution MEPC.320(74), https://wwwcdn.imo.org/localresources/en/OurWork/Environment/Documents/MEPC.320(74).pdf (last access: 20.01.2023), 2019.

IMO (International Maritime Organization): Marine Environment Protection Committee (MEPC) – 79th session, 12-16 December 2022, https://www.imo.org/en/MediaCentre/MeetingSummaries/Pages/MEPC-79th-session.aspx (last access: 16.01.23).

Jägerbrand, A. K., Brutemark, A., Barthel Svedén, J., and Gren, I.-M.: A review on the environmental impacts of shipping on aquatic and nearshore ecosystems, Sci. Total Environ., 695, 133637, https://doi.org/10.1016/j.scitotenv.2019.133637, 2019.

Jalkanen, J.-P., Johansson, L., Kukkonen, J., Brink, A., Kalli, J., and Stipa, T.: Extension of an assessment model of ship traffic exhaust emissions for particulate matter and carbon monoxide, Atmos. Chem. Phys., 12, 2641–2659, https://doi.org/10.5194/acp-12-2641-2012, 2012.

Jalkanen, J.-P., Brink, A., Kalli, J., Pettersson, H., Kukkonen, J., and Stipa, T.: A modelling system for the exhaust emissions of marine traffic and its application in the Baltic Sea area, Atmos. Chem. Phys., 9, 9209–9223, https://doi.org/10.5194/acp-9-9209-2009, 2009.

Johansson, L., Jalkanen, J.-P., Kalli, J., and Kukkonen, J.: The evolution of shipping emissions and the costs of regulation changes in the northern EU area, Atmos. Chem. Phys., 13, 11375–11389, https://doi.org/10.5194/acp-13-11375-2013, 2013.

Johansson, L., Jalkanen, J.-P., and Kukkonen, J.: Global assessment of shipping emissions in 2015 on a high spatial and temporal resolution, Atmos. Environ., 167, 403-415, https://doi.org/10.1016/j.atmosenv.2017.08.042, 2017.

Jiang, W., Smyth, S., Giroux, É., Roth, H., and Yin, D.: Differences between CMAQ fine mode particle and PM2.5 concentrations and their impact on model performance evaluation in the lower Fraser valley, Atmospheric Environment, 40(26), 4973-4985, https://doi.org/10.1016/j.atmosenv.2005.10.069, 2006.

Jimenez, J. L., Canagaratna, M. R., Donahue, N. M., Prevot, A. S. H., Zhang, Q., Kroll, J. H., DeCarlo, P. F., Allan, J. D., Coe, H., Ng, N. L., Aiken, A. C., Docherty, K. S., Ulbrich, I. M., Grieshop, A. P., Robinson, A. L., Duplissy, J., Smith, J. D., Wilson, K. R., Lanz, V. A., Hueglin, C., Sun, Y. L., Tian, J., Laaksonen, A., Raatikainen, T., Rautiainen, J., Vaattovaara, P., Ehn, M., Kulmala, M., Tomlinson, J. M., Collins, D. R., Cubison, M. J., Dunlea, E. J., Huffman, J. A., Onasch, T. B., Alfarra, M. R., Williams, P. I., Bower, K., Kondo, Y., Schneider, J., Drewnick, F., Borrmann, S., Weimer, S., Demerjian, K., Salcedo, D., Cottrell, L., Griffin, R., Takami, A., Miyoshi, T., Hatakeyama, S., Shimono, A., Sun, J. Y., Zhang, Y. M., Dzepina, K., Kimmel, J. R., Sueper, D., Jayne, J. T., Herndon, S. C., Trimborn, A. M., Williams, L. R., Wood, E. C., Middlebrook, A. M., Kolb, C. E., Baltensperger, U., and Worsnop, D. R.: Evolution of organic aerosols in the atmosphere, Science, 326(5959), 1525-1529, https://doi.org/10.1126/science.1180353, 2009.

Jonson, J. E., Gauss, M., Schulz, M., Jalkanen, J.-P., and Fagerli, H.: Effects of global ship emissions on European air pollution levels, Atmos. Chem. Phys., 20, 11399–11422, https://doi.org/10.5194/acp-20-11399-2020, 2020.

Karamfilova, E.: BRIEFING Implementation Appraisal, Revision of the EU Ambient Air Quality Directives, EPRS European Parliamentary Research Service, https://www.europarl.europa.eu/RegData/etudes/BRIE/2022/734679/EPRS_BRI(2022)734679_EN.pdf, 2022.

Karl, M., Bieser, J., Geyer, B., Matthias, V., Jalkanen, J.-P., Johansson, L., and Fridell, E.: Impact of a nitrogen emission control area (NECA) on the future air quality and nitrogen deposition to seawater in the Baltic Sea region, Atmos. Chem. Phys., 19, 1721–1752, https://doi.org/10.5194/acp-19-1721-2019, 2019.

Kelly, J. T., Bhave, P. V., Nolte, C. G., Shankar, U., and Foley, K. M.: Simulating emission and chemical evolution of coarse sea-salt particles in the Community Multiscale Air Quality (CMAQ) model, Geosci. Model Dev., 3, 257–273, https://doi.org/10.5194/gmd-3-257-2010, 2010.

Kiesewetter, G., Schoepp, W., Heyes, C., and Amann, M.: Modelling PM2.5 impact indicators in Europe: Health effects and legal compliance, Environ. Modell Softw., 74, 201-211, https://doi.org/10.1016/j.envsoft.2015.02.022, 2015.

Klingmüller, K., Metzger, S., Abdelkader, M., Karydis, V. A., Stenchikov, G. L., Pozzer, A., and Lelieveld, J.: Revised mineral dust emissions in the atmospheric chemistry-climate model EMAC (based on MESSy 2.52), Geosci. Model Dev, https://doi.org/10.5194/gmd-2017-160, 2017.

Kleijn, D., Kohler, F., Báldi, A., Batáry, P., Concepción, E. D., Clough, Y., Díaz, M., Gabriel, D., Holzschuh, A., Knop, E., Kovács, A., Marshall, E. J. P., Tscharntke, T., and Verhulst, J.: On the relationship between farmland biodiversity and land-use intensity in Europe, Proc. R. Soc., 276(1658), https://doi.org/10.1098/rspb.2008.1509, 2009.

Klimont, Z., Kupiainen, K., Heyes, C., Purohit, P., Cofala, J., Rafaj, P., Borken-Kleefeld, J., and Schöpp, W.: Global anthropogenic emissions of particulate matter including black carbon, Atmos. Chem. Phys., 17, 8681–8723, https://doi.org/10.5194/acp-17-8681-2017, 2017.

Kranenburg, R., Segers, A. J., Hendriks, C., and Schaap, M.: Source apportionment using LOTOS-EUROS: module description and evaluation, Geosci. Model Dev., 6, 721–733, https://doi.org/10.5194/gmd-6-721-2013, 2013.

Krupa, S.V.: Effects of atmospheric ammonia (NH3) on terrestrial vegetation: a review, Environ. Pollut.,124(2), 179-221, https://doi.org/10.1016/s0269-7491(02)00434-7, 2003.

Kuenen, J., Dellaert, S., Visschedijk, A., Jalkanen, J.-P., Super, I., and Denier van der Gon, H.: CAMS-REG-v4: a state-of-the-art high-resolution European emission inventory for air quality modelling, Earth Syst. Sci. Data, 14, 491–515, https://doi.org/10.5194/essd-14-491-2022, 2022.

Kuenen, J. J. P., Visschedijk, A. J. H., Jozwicka, M., and Denier van der Gon, H. A. C.: TNO-MACC_II emission inventory; a multi-year (2003–2009) consistent high-resolution European emission inventory for air quality modelling, Atmos. Chem. Phys., 14, 10963–10976, https://doi.org/10.5194/acp-14-10963-2014, 2014.

Loosmore, G. A. and Cederwall, R. T.: Precipitation scavenging of atmospheric aerosols for emergency response applications: testing an updated model with new real-time data, Atmospheric Environment, 38(7), 993-1003, https://doi.org/10.1016/j.atmosenv.2003.10.055, 2004.

Mallet, M. D., D'Anna, B., Même, A., Bove, M. C., Cassola, F., Pace, G., Desboeufs, K., Di Biagio, C., Doussin, J.-F., Maille, M., Massabò, D., Sciare, J., Zapf, P., di Sarra, A. G., and Formenti, P.: Summertime surface PM1 aerosol composition and size by source region at the Lampedusa island in the central Mediterranean Sea, Atmos. Chem. Phys., 19, 11123–11142, https://doi.org/10.5194/acp-19-11123-2019, 2019.

Manders, A. M. M., Builtjes, P. J. H., Curier, L., van der Denier Gon, H. A. C., Hendriks, C., Jonkers, S., Kranenburg, R., Kuenen, J. J. P., Segers, A. J., Timmermans, R. M. A., Visschedijk, A. J. H., Wichink Kruit, R. J., van Pul, W. A. J., Sauter, F. J., van der Swaluw, E., Swart, D. P. J., Douros, J., Eskes, H., van Meijgaard, E., van Ulft, B., van Velthoven, P., Banzhaf, S., Mues, A. C., Stern, R., Fu, G., Lu, S., Heemink, A., van Velzen, N., and Schaap, M.: Curriculum vitae of the LOTOS–EUROS (v2.0) chemistry transport model, Geosci. Model Dev., 10, 4145–4173, https://doi.org/10.5194/gmd-10-4145-2017, 2017.

Manders-Groot, A., Segers, A., and Jonkers, S.: LOTOS-EUROS v2.0 Reference Guide, Report, https://lotos-euros.tno.nl/media/10360/reference_guide_v2-0_r10898.pdf, 2016.

Marmer, E. and Langmann, B.: Impact of ship emissions on the Mediterranean summertime pollution and climate: A regional model study, Atmos. Environ., 39(26), 4659-4669, https://doi.org/10.1016/j.atmosenv.2005.04.014, 2005.

980 Mårtensson, E. M., Nilsson, E. D., Leeuw, G. de, Cohen, L. H., and Hansson, H.-C.: Laboratory simulations and parameterization of the primary marine aerosol production, J. Geophys. Res., 108(D9), 4297, https://doi.org/10.1029/2002JD002263, 2003.

Marticorena, B. and Bergametti, G.: Modelling the atmospheric dust cycle: 1. Design of a soil drived dust emission scheme., J. Geophys. Res., 100, 16415–16430, doi:10.1029/95jd00690, 1995.

985 Marticorena, B., Bergametti, G., Aumont, B., Callot, Y., N'Doume,́ C., and Legrand, M.: Modelling the atmospheric dust cycle: 2. Simulation of Saharan dust sources, J. Geophys. Res., 102, 4387– 4404, 1997.

Matthias, V., Bewersdorff, I., Aulinger, A., and Quante, M.: The contribution of ship emissions to air pollution in the North Sea regions, Environ. Pollut., 158(6), 2241-2250, https://doi.org/10.1016/j.envpol.2010.02.013, 2010.

Matthias, V.: The aerosol distribution in Europe derived with the Community Multiscale Air Quality (CMAQ) model: 990 comparison to near surface in situ and sunphotometer measurements, Atmos. Chem. Phys., 8, 5077–5097, https://doi.org/10.5194/acp-8-5077-2008, 2008.

Menut, L., Bessagnet, B., Khvorostyanov, D., Beekmann, M., Blond, N., Colette, A., Coll, I., Curci, G., Foret, G., Hodzic, A., Mailler, S., Meleux, F., Monge, J.-L., Pison, I., Siour, G., Turquety, S., Valari, M., Vautard, R., and Vivanco, M. G.: CHIMERE 2013: A model for regional atmospheric composition modelling, Geosci. Model Dev., 6, 981–1028, 995 https://doi.org/10.5194/gmd-6-981-2013, 2013.

Monahan, E. C., Spiel, D. E., and Davidson, K. L.: A Model of Marine Aerosol Generation Via Whitecaps and Wave Disruption, OCSL, 2,https://doi.org/10.1007/978-94-009-4668-2_16, 1986.

Nenes, A., Pandis, S. N., and Pilinis, C.: ISORROPIA: A New Thermodynamic Equilibrium Model for Multiphase Multicomponent Inorganic Aerosols, Aquat. Geochem., 4, 123–152, https://doi.org/10.1023/A:1009604003981, 1998.

1000 Nunes, R. A. O., Alvim-Ferraz, M. C. M., Martins, F. G., Calderay-Cayetano, F., Durán-Grados, V., Moreno-Gutiérrez, J., Jalkanen, J.-P., Hannuniemi, H., and Sousa, S. I. V.: Shipping emissions in the Iberian Peninsula and the impacts on air quality, Atmos. Chem. Phys., 20, 9473–9489, https://doi.org/10.5194/acp-20-9473-2020, 2020.

Ovadnevaite, J., Manders, A., Leeuw, G. de, Ceburnis, D., Monahan, C., Partanen, A.-I., Korhonen, H., and O'Dowd, C. D.: A sea spray aerosol flux parameterization encapsulating wave state, Atmos. Chem. Phys., 14, 1837–1852, 1005 https://doi.org/10.5194/acp-14-1837-2014, 2014.

Palacios-Peña, L.; Lorente-Plazas, R.; Montávez, J.P.; Jiménez-Guerrero, P.: Saharan Dust Modeling Over the Mediterranean Basin and Central Europe: Does the Resolution Matter? Front. Earth Sci., 7(290), doi: 10.3389/feart.2019.00290, 2019.

Pandolfi, M., Gonzalez-Castanedo, Y., Alastuey, A., La Rosa, J. D. de, Mantilla, E., La Campa, A. S. de, Querol, X., Pey, J., Amato, F., and Moreno, T.: Source apportionment of PM(10) and PM(2.5) at multiple sites in the strait of Gibraltar by PMF: 1010 impact of shipping emissions, Environ. Sci. Pollut. Res.18, 260–269, https://doi.org/10.1007/s11356-010-0373-4, 2011.

Park, S.-K., Marmur, A., Kim, S. B., Di Tian, Hu, Y., McMurry, P. H., and Russell, A. G.: Evaluation of Fine Particle Number Concentrations in CMAQ, Aerosol Sci. Technol., 40(11), 985-996, https://doi.org/10.1080/02786820600907353, 2006.

Pepe, N., Pirovano, G., Balzarini, A., Toppetti, A., Riva, G. M., Amato, F., and Lonati, G.: Enhanced CAMx source apportionment analysis at an urban receptor in Milan based on source categories and emission regions, Atmos. Environ. X, 1015 2,100020, https://doi.org/10.1016/j.aeaoa.2019.100020, 2019.

Pleim, J. E., Xiu, A., Finkelstein, P. L., and Otte, T. L.: A Coupled Land-Surface and Dry Deposition Model and Comparison to Field Measurements of Surface Heat, Moisture, and Ozone Fluxes, Water Air Soil Pollut.: Focus, 1, 243–252, https://doi.org/10.1023/A:1013123725860, 2001.

Prati, M. V., Costagliola, M. A., Quaranta, F., and Murena, F.: Assessment of ambient air quality in the port of Naples, J. Air Waste Manag. Assoc., 65, 970-979, https://doi.org/10.1080/10962247.2015.1050129, 2015.

Pye, H. O. T., Murphy, B. N., Xu, L., Ng, N. L., Carlton, A. G., Guo, H., Weber, R., Vasilakos, P., Appel, K. W., Budisulistiorini, S. H., Surratt, J. D., Nenes, A., Hu, W., Jimenez, J. L., Isaacman-VanWertz, G., Misztal, P. K., and Goldstein, A. H.: On the implications of aerosol liquid water and phase separation for organic aerosol mass, Atmos. Chem. Phys., 17, 343–369, https://doi.org/10.5194/acp-17-343-2017, 2017.

Pye, H. O. T. and Pouliot, G. A.: Modeling the role of alkanes, polycyclic aromatic hydrocarbons, and their oligomers in secondary organic aerosol formation, Environ. Sci. Technol., 6041-6047, https://doi.org/10.1021/es300409w, 2012.

Ramboll Environment and Health: User's Guide COMPREHENSIVE AIR QUALITY MODEL WITH EXTENSIONS: Version 7.10, User's Guide, https://camx-wp.azurewebsites.net/Files/CAMxUsersGuide_v7.10.pdf, 2020.

Reichle, L. J., Cook, R., Yanca, C. A., and Sonntag, D. B.: Development of organic gas exhaust speciation profiles for nonroad spark-ignition and compression-ignition engines and equipment, J. Air Waste Manag. Assoc., 65(10), 1185–1193, https://doi.org/10.1080/10962247.2015.1020118, 2015.

Remke, E., Brouwer, E., Kooijman, A., Blindow, I., Esselink, H., and Roelofs, J. G. M.: Even low to medium nitrogen deposition impacts vegetation of dry, coastal dunes around the Baltic Sea, Environ. Pollut., 157(3), 792-800, https://doi.org/10.1016/j.envpol.2008.11.020, 2009.

Riccio, A., Ciaramella, A., Giunta, G., Galmarini, S., Solazzo, E., and Potempski, S.: On the systematic reductionof data complexity in multimodel atmospheric dispersion ensemble modeling, J. Geophys. Res., 117, D05314, https://doi.org/10.1029/2011JD016503, 2012.

Robinson, A. L., Donahue, N. M., Shrivastava, M. K., Weitkamp, E. A., Sage, A. M., Grieshop, A. P., Lane, T. E., Pierce, J. R., and Pandis, S. N.: Rethinking organic aerosols: semivolatile emissions and photochemical aging, Science, 315(5816), https://doi.org/10.1126/science.1133061, 2007.

Roselle, S. J. and Binkowski, F. S.: Cloud Dynamics and Chemistry: Chapter 11, https://www.cmascenter.org/cmaq/science_documentation/pdf/ch11.pdf, 1999.

Schaap, M., van Loon, M., ten Brink, H. M., Dentener, F. J., and Builtjes, P. J. H.: Secondary inorganic aerosol simulations for Europe with special attention to nitrate, Atmos. Chem. Phys., 4, 857–874, https://doi.org/10.5194/acp-4-857-2004, 2004.

Schaap, M., Manders, A.M.M., Hendriks, E.C.J., Cnossen, J.M., Segers, A.J.S., Denier van der Gon, H.A.C., Jozwicka, M., Sauter, F., Velders, G., Matthijsen, J., Builtjes, P.J.H.: Regional modelling of particulate matter for the Netherlands. Tech.rep. Netherlands Environmental Assessment Agency (PBL). https://www.pbl.nl/sites/default/files/downloads/500099008_0.pdf, 2009.

Schembari, C., Cavalli, F., Cuccia, E., Hjorth, J., Calzolai, G., Pérez, N., Pey, J., Prati, P., and Raes, F.: Impact of a European directive on ship emissions on air quality in Mediterranean harbours, Atmospheric Environment, 61, 661-669, https://doi.org/10.1016/j.atmosenv.2012.06.047, 2012.

Schober, P., Boer, C., and Schwarte, L. A.: Correlation Coefficients: Appropriate Use and Interpretation, Anesth. Analg., 126(5), 1763-1768, https://doi.org/10.1213/ANE.0000000000002864, 2018.

Seinfeld, J.H. and Pandis, S.N. (2006) Atmospheric Chemistry and Physics: From Air Pollution to Climate Change. 2nd Edition, John Wiley & Sons, New York, 2006.

Simpson, D., Benedictow, A., Berge, H., Bergström, R., Emberson, L. D., Fagerli, H., Flechard, C. R., Hayman, G. D., Gauss, M., Jonson, J. E., Jenkin, M. E., Nyíri, A., Richter, C., Semeena, V. S., Tsyro, S., Tuovinen, J.-P., Valdebenito, Á., and Wind, P.: The EMEP MSC-W chemical transport model – technical description, Atmos. Chem. Phys., 12, 7825–7865, https://doi.org/10.5194/acp-12-7825-2012, 2012.

Simpson, D., Bergström, R., Briolat, A., Imhof, H., Johansson, J., Priestley, M., and Valdebenito, A.: GenChem v1.0 – a chemical pre-processing and testing system for atmospheric modelling, Geosci. Model Dev., 13, 6447–6465, https://doi.org/10.5194/gmd-13-6447-2020, 2020.

Sippula, O., Stengel, B., Sklorz, M., Streibel, T., Rabe, R., Orasche, J., Lintelmann, J., Michalke, B., Abbaszade, G., Radischat, C., Gröger, T., Schnelle-Kreis, J., Harndorf, H., and Zimmermann, R.: Particle emissions from a marine engine: chemical composition and aromatic emission profiles under various operating conditions, Environ. Sci. Technol., 48(19), 11721–11729, https://doi.org/10.1021/es502484z, 2014.

Solazzo, E., Bianconi, R., Pirovano, G., Matthias, V., Vautard, R., Moran, M. D., Wyat Appel, K., Bessagnet, B., Brandt, J., Christensen, J. H., Chemel, C., Coll, I., Ferreira, J., Forkel, R., Francis, X. V., Grell, G., Grossi, P., Hansen, A. B., Miranda, A. I., Nopmongcol, U., Prank, M., Sartelet, K. N., Schaap, M., Silver, J. D., Sokhi, R. S., Vira, J., Werhahn, J., Wolke, R., Yarwood, G., Zhang, J., Rao, S. T., and Galmarini, S.: Operational model evaluation for particulate matter in Europe and North America in the context of AQMEII, Atmos. Environ., 53, 75-92, https://doi.org/10.1016/j.atmosenv.2012.02.045, 2012.

Solazzo, E., Riccio, A., Kioutsioukis, I., and Galmarini, S.: Pauci ex tanto numero: reduce redundancy in multi-model ensembles, Atmos. Chem. Phys., 13, 8315–8333, https://doi.org/10.5194/acp-13-8315-2013, 2013.

Solazzo, E., Riccio, A., van Dingenen, R., Valentini, L., and Galmarini, S.: Evaluation and uncertainty estimation of the impact of air quality modelling on crop yields and premature deaths using a multi-model ensemble, Sci. Total Environ., 633, 1437–1452, https://doi.org/10.1016/j.scitotenv.2018.03.317, 2018.

Song, S.-K. and Shon, Z.-H.: Current and future emission estimates of exhaust gases and particles from shipping at the largest port in Korea, Environ. Sci. Pollut. Res., 21, 6612–6622, https://doi.org/10.1007/s11356-014-2569-5, 2014.

Sotiropoulou, R. E. P. and Tagaris, E.: Impact of Shipping Emissions on European Air Quality, In: Karacostas, T., Bais, A., Nastos, P. (eds) Perspectives on Atmospheric Sciences, Springer Atmospheric Sciences, https://doi.org/10.1007/978-3-319-35095-0_149, 2017.

Tadic, I., Crowley, J. N., Dienhart, D., Eger, P., Harder, H., Hottmann, B., Martinez, M., Parchatka, U., Paris, J.-D., Pozzer, A., Rohloff, R., Schuladen, J., Shenolikar, J., Tauer, S., Lelieveld, J., and Fischer, H.: Net ozone production and its relationship to nitrogen oxides and volatile organic compounds in the marine boundary layer around the Arabian Peninsula, Atmos. Chem. Phys., 20, 6769–6787,, https://doi.org/10.5194/acp-20-6769-2020, 2020.

Tuccella, P., Menut, L., Briant, R., Deroubaix, A., Khvorostyanov, D., Mailler, S., Siour, G., and Turquety, S.: Implementation of Aerosol-Cloud Interaction within WRF-CHIMERE Online Coupled Model: Evaluation and Investigation of the Indirect Radiative Effect from Anthropogenic Emission Reduction on the Benelux Union, Atmosphere, 10(1), 20, https://doi.org/10.3390/atmos10010020, 2019.

Večeřa, Z., Mikuška, P., Smolík, J., Eleftheriadis, K., Bryant, C., Colbeck, I., and Lazaridis, M.: Shipboard Measurements of Nitrogen Dioxide, Nitrous Acid, Nitric Acid and Ozone in the Eastern Mediterranean Sea, Water Air Soil Pollut: Focus, 8, 117–125, https://doi.org/10.1007/s11267-007-9133-y, 2008.

Viana, M., Amato, F., Alastuey, A., Querol, X., Moreno, T., Dos Santos, S. G., Herce, M. D., and Fernández-Patier, R.: Chemical tracers of particulate emissions from commercial shipping, Environ. Sci. Technol., 43(19), 7472–7477, https://doi.org/10.1021/es901558t, 2009.

Viana, M., Hammingh, P., Colette, A., Querol, X., Degraeuwe, B., Vlieger, I. d., and van Aardenne, J.: Impact of maritime transport emissions on coastal air quality in Europe, Atmos. Environ., 90, 96-105, https://doi.org/10.1016/j.atmosenv.2014.03.046, 2014.

Viana, M., Rizza, V., Tobías, A., Carr, E., Corbett, J., Sofiev, M., Karanasiou, A., Buonanno, G., and Fann, N.: Estimated health impacts from maritime transport in the Mediterranean region and benefits from the use of cleaner fuels, Environ. Internat., 138,105670, https://doi.org/10.1016/j.envint.2020.105670, 2020.

Wei, H., Feng, Y., Liang, F., Cheng, W., Wu, X., Zhou, R., and Wang, Y.: Role of oxidative stress and DNA hydroxymethylation in the neurotoxicity of fine particulate matter, Toxicology, 380, 94-103, https://doi.org/10.1016/j.tox.2017.01.017, 2017.

Wesely, M. L.: Parameterization of surface resistances to gaseous dry deposition in regional-scale numerical models, Atmos. Environ., 23 (6), 1293-1304, https://doi.org/10.1016/0004-6981(89)90153-4, 1989.

Whitten, G. Z., H. Hogo, and J.P. Killus, The carbon-bond mechanism: A condensed kinetic mechanism for photochemical smog, Environ. Sci. Technol., 18, 280-87, 1980.

WHO global air quality guidelines. Particulate matter (PM¬2.5 and PM10), ozone, nitrogen dioxide, sulphur dioxide and carbon monoxide, Geneva: World Health Organization, https://apps.who.int/iris/bitstream/handle/10665/345329/9789240034228-eng.pdf, 2021.

Wiedinmyer, C., S. K. Akagi, R. J. Yokelson, L. K. Emmons, J. A. Al-Saadi, J. J. Orlando and A. J. Soja (2011). "The Fire INventory from NCAR (FINN): a high resolution global model to estimate the emissions from open burning." Geoscientific Model Development **4**(3): 625-641.

Wolff, V., Trebs, I., Ammann, C., and Meixner, F. X.: Aerodynamic gradient measurements of the NH3-HNO3-NH4NO3 triad using a wet chemical instrument: an analysis of precision requirements and flux errors, Atmos. Meas. Tech., 3, 187–208, https://doi.org/10.5194/amt-3-187-2010, 2010.

Zender, C., Bian, H., and Newman, D.: Mineral Dust Entrainmentand Deposition (DEAD) model: Description and 1990s dust climatology., J. Geophys. Res., 108, 4416–4437, doi:10.1029/2002jd002775, 2003.

Zhang, L., Brook, J. R., and Vet, R.: A revised parameterization for gaseous dry deposition in air-quality models, Atmos. Chem. Phys., 3, 2067–2082, https://doi.org/10.5194/acp-3-2067-2003, 2003.

Zhong, Q., Shen, H., Yun, X., Chen, Y., Ren, Y.'a., Xu, H., Shen, G., Du, W., Meng, J., Li, W., Ma, J., and Tao, S.: Global Sulfur Dioxide Emissions and the Driving Forces, Environ. Sci. Technol., 54(11), 6508–6517, https://doi.org/10.1021/acs.est.9b07696, 2020.

Appendix A:

Figure A1: Domains and measurement stations. Red trapeze displays the 12 x 12 km² domain, blue dots are locations of measurement stations. On bottom left the larger 36 x 36 km² domain is displayed.

Appendix B:

Table B1: detailed overview of monitoring stations

Name	Code	Country	Latitude	Longitude	Ele-vation	Station Type	Data Points	Measured Pollutants
Vlora	al0204a	Albania	40.40309	19.4862	25	urban background	6850	benzene, CO, NO_2, NO_x, O_3, PM_{10}, $PM_{2.5}$, SO_2
Shkoder	al0206a	Albania	42.3139	19.52342	13	urban background	7536	CO, NO_2, NO_x, O_3, PM_{10}, $PM_{2.5}$, SO_2
Els Torms	es0014r	Spain	41.39389	0.73472	470	rural background	8549	NO, NO_2, NO_x, O_3, SO_2, $PM_{2.5}$
Marseille 5 Avenues	fr03043	France	43.30607	5.395794	73	urban background	8585	NO_2, O_3, PM_{10}, $PM_{2.5}$, SO_2
Gauzy	fr08614	France	43.8344	4.374219	40	urban background	8406	NO_2, O_3, PM_{10}, $PM_{2.5}$
Cannes Broussilles	fr24009	France	43.5625	7.007222	71	urban background	8587	NO_2, O_3, PM_{10}, $PM_{2.5}$
Manosque	fr24018	France	43.83527	5.785831	385	urban background	8517	NO_2, O_3, PM_{10}, $PM_{2.5}$
Nice Arson	fr24036	France	43.70207	7.286264	11	urban background	8701	NO_2, O_3, PM_{10}, $PM_{2.5}$
Bastia Montesoro	fr41017	France	42.67134	9.434644	47	rural background	8626	NO_2, O_3, $PM_{2.5}$
Lykovrysi	gr0035a	Greece	38.06963	23.77689	210	suburban background	6719	NO_2, NO_2, $PM_{2.5}$, O_3
Priolo	it0614a	Italy	37.15612	15.19087	35	urban background	7902	NO_2, $PM_{2.5}$, benzene, SO_2
Leonessa	it0989a	Italy	42.5725	12.96194	948	urban background	8207	NO_2, $PM_{2.5}$, O_3
Gherardi	it1179a	Italy	44.83972	11.96111	-2	rural background	8269	NO_x, $PM_{2.5}$, NO_2, O_3

Teatro d'Annunzio	it1423a	Italy	42.45639	14.23472	4	urban background	8135	NO_2, O_3, PM_{10}, $PM_{2.5}$, SO_2, benzene, CO
Cenps7	it1576a	Italy	39.20333	8.386111	25	suburban background	7968	CO, NO_2, SO_2, $PM_{2.5}$
Lecce - S.M. Cerrate	it1665a	Italy	40.45889	18.11611	10	rural background	7290	NO_2, O_3, $PM_{2.5}$
Brindisi Via Magellano	it1702a	Italy	40.65083	17.94361	10	suburban background	7904	NO_2, PM_{10}, $PM_{2.5}$
Genga - Parco Gola della Rossa	it1773a	Italy	43.46806	12.95222	550	rural background	5310	NO_2, O_3, PM_{10}, $PM_{2.5}$, SO_2, benzene, CO
Civitanova Ippodromo S. Marone	it1796a	Italy	43.33556	13.67472	110	rural background	6699	NO_2, NO_x, O_3, PM_{10}, $PM_{2.5}$, benzene
Ancona Cittadella	it1827a	Italy	43.61167	13.50861	100	urban background	5985	NO_2, O_3, PM_{10}, $PM_{2.5}$, benzene, CO, SO_2
Schivenoglia	it1865a	Italy	44.99694	11.07083	16	rural background	8325	NO_2, NO_x, O_3, SO_2, benzene, $PM_{2.5}$
San Rocco	it1914a	Italy	44.87306	10.66389	22	rural background	8398	NO_2, NO_x, O_3, $PM_{2.5}$
Locri	it1940a	Italy	38.22976	16.25518	11	urban background	8509	NO_2, O_3, SO_2, benzene, CO, $PM_{2.5}$
Censa3	it1947a	Italy	39.06667	9.008889	56	urban background	8169	NO_2, SO_2, benzene, $PM_{2.5}$
Stadio Casardi	it2003a	Italy	41.31667	16.28611	15	urban background	8391	NO_2, O_3, benzene, $PM_{2.5}$
Ceglie Messapica	it2148a	Italy	40.64917	17.5125	100	suburban background	8393	NO_2, PM_{10}, $PM_{2.5}$, SO_2, CO, benzene